TÉCNICO LISBOA

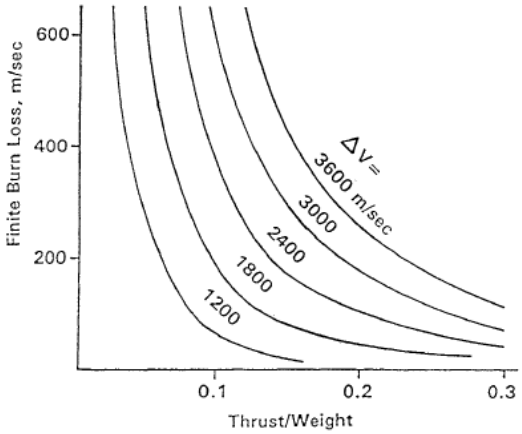

Finite burn losses in spacecraft maneuvers revisited

José Carlos Franco Confraria

Thesis to obtain the Master of Science Degree in

Aerospace Engineering

Supervisor: Prof. Paulo Jorge Soares Gil

Examination Committee

Chairperson: Prof. Filipe Szolnoky Ramos Pinto Cunha
Supervisor: Prof. Paulo Jorge Soares Gil
Member of the Committee: Prof. João Manuel Gonçalves de Sousa Oliveira

November 2020

Dedico à minha familia e amigos.

Acknowledgments

Quero agradecer ao Orientador Paulo Gil pela sua capacidade de orientação e sobretudo interesse, e ao Professor André Marta por disponibilizar uma template em latex para teses. E a todos os que me apoiaram nesta fase.

Resumo

Neste trabalho é realizada uma avaliação das denominadas perdas por gravidade em manobras de impulso considerável, que costumam ser aproximadas por manobras instantâneas em estudos preliminares. Para tal foi utilizado um método de optimização, *direct shooting*. Foram estudados três tipos de manobras: direção da propulsão constante; rotação constante e propulsão alinhada com a velocidade.

Os vários casos são estudados em função do impulso especifico e razão força/peso, bem como analizadas as suas vantagens e desvantagens relativas. O caso que apresenta menor desempenho é o de propulsão com direção constante, como seria de esperar, sendo que os resultados obtidos apresentam algumas surpresas, que são discutidas.

Os resultados são também comparados com uma aproximação conhecida da literatura e estudadas as consequências de utilizar manobras de elevação de apogeu para minimizar as perdas por gravidade.

Palavras-chave: perdas por gravidade, multiplas manobras, direct shooting

Abstract

In this work, an evaluation of losses due to gravity and steering is done for high thrust spacecraft maneuvers, which are normally approximated as instantaneous maneuvers on preliminary studies. For this purpose an optimization method was used, the so called direct shooting. Three steering cases were studied: constant thrust direction, constant rotation, and thrust aligned with velocity.

Then, the various steering cases are studied in function of the specific impulse and thrust over weight. The case with the least performance is the case of constant thrust direction, as expected, while the results obtained show some surprises, which are discussed.

The results are also compared to a known approximation of the literature where the losses are upper bounded. At the end as an alternative to direct maneuvers, the consequences of multiple apogee raising maneuvers to minimize the gravity losses are studied.

Keywords: gravity losses, multiple maneuvers, direct shooting

Contents

List of Tables

List of Figures

Nomenclature

Greek symbols

α	Initial angle direction
$\dot{\alpha}$	angle rotation
μ	Standard gravitational parameter

Roman symbols

Ω	Right ascension of ascending node
ω	argument of perigee
a	Semimajor axis
$a(t)$	Acceleration
C_3	Characteristic energy
e	Eccentricity
h	Angular momentum
i	inclination
I_{sp}	Specific Impulse
m_i	Initial mass
m_p	Propellant mass
r	Radius magnitude
T	Thrust magnitude
t	Time
v	Velocity magnitude
W_0	Initial weight
w_s	Schuler frequency

Subscripts

∞	asymptotic
x, y, z	Cartesian components in the inertial frame of the main body

Glossary

GMAT General Mission Analysis Tool. xxi

SQP Sequential Quadratic Programing. xxi

Chapter 1

Introduction

1.1 Objectives and Motivation

In this thesis the problem of determining gravity losses for a generalized spacecraft maneuver is analysed. Heuristics that estimate these losses are reviewed to confirm their validity by comparison with numerical calculations and a procedure to minimize losses with a multi-impulse maneuver is presented.

1.2 Spacecraft maneuvering

In preliminary mission design a first approximation of the trajectories must be determined, while the spacecraft hardware is yet to be completely developed. Since high accuracy is not required, some simplifications and assumptions can be used. These assumptions involve simplifying orbital maneuvers to determine a delta-v budget, in which an error is introduced that must be evaluated and taken into account [1]. It is important to have good initial guesses for mission design, as better approximations can yield faster convergence of the orbit design and other systems such as the propulsion system.

1.2.1 Types of maneuvers

Orbital maneuvers can be divided in two types: high thrust maneuvers, which typically last a few minutes and are approximated as instantaneous, and the so called continuous thrust maneuvers, where the thrust is very small but the thrusters are highly efficient.

The high thrust maneuvers are produced by chemical energy, where the engines can be solid, liquid (bipropellant or monopropellant) or hybrid. Other options, such as nuclear thermal engines, which are being studied but still have not been used. Typically, these engines perform maneuvers such as: Hohmann transfers, apogee raisings, apogee maneuvers or interplanetary injections. Continuous thrust maneuvers are propelled by electric energy (for example: ion gridded thrusters, arcjets, resistojets and others) generally for long maneuvers where the spacecraft is small and higher efficiency is important. This work focus on finite high thrust maneuvers produced by chemical thrusters.

High thrust maneuvers are typically performed by interplanetary probes and upper stages. Such spacecrafts typically use bipropellant liquid thrusters as their main engine with a specific impulse around 300 s and thrust magnitude on the order of 500 N. These thrusters are used for the main maneuvers such as: planet insertion maneuver or apogee maneuver. Upper stages use liquid propellant engines with a typical specific impulse from 350 s to 450 s and thrust levels from 20 kN to 90 kN [2] [3]. In this work both upper stages and small spacecraft are studied for a wide range of impulsive maneuvers.

1.2.2 Impulsive Approximation

In preliminary mission analysis, high thrust maneuvers, are often approximated as an instantaneous change in the velocity. This is convenient because it separates the problem of the maneuver from the problem of specifying the spacecraft, but implies an error, usually fairly small, as the actual burns typically occur only during a small part of the orbital period [1]. This approximation considers that the spacecraft changes from one state to another instantly, simply connecting two ordinary two-body problems (another approximation), making the problem description simple, with only two orbits and a change of the velocity vector in a point in space, Δv.The calculated Δv can be used to estimate the propellant mass needed for a given thruster and payload mass [4].

Nevertheless, the impulsive approximation is only valid to a certain degree. The burn always occurs in a finite interval of time and the real maneuver is different from the instantaneous one. The Δv from both is therefore different and so will be the predicted propellant for the maneuver.

1.2.3 High thrust finite burn maneuver

To gain insight about the shortcomings of an impulsive approximation, let us consider a simplified apoapsis raising maneuver that can be thought of as an Hohmann transfer. The spacecraft starts from a circular or elliptical orbit and wants to reach an elliptical orbit with the apoapsis equal to the radius of the final orbit. Prior to the burn, the spacecraft is on the initial orbit, and a constant thrust is applied to reach the desired orbit as shown in figure 1.1.

On an impulsive approximation, when the ”burn” occurs, that point simply becomes the periapsis of the new orbit. The real maneuver always takes a certain amount of time and that causes the so called finite burn losses. In the example, we can observe that:

- The burn does not occur solely at the periapsis (one point in space), where the gravity loss (explained bellow) is minimal, but also around it;
- The required direction of the thrust during the burn for achieving the desired final orbit is non-trivial and may be non-optimal, leading to steering losses (explained bellow);
- The spacecraft mass is decreasing as the propellant mass is expelled at a certain mass flow rate and the thrust's acceleration varies (depending on how the mass flow rate is controlled);

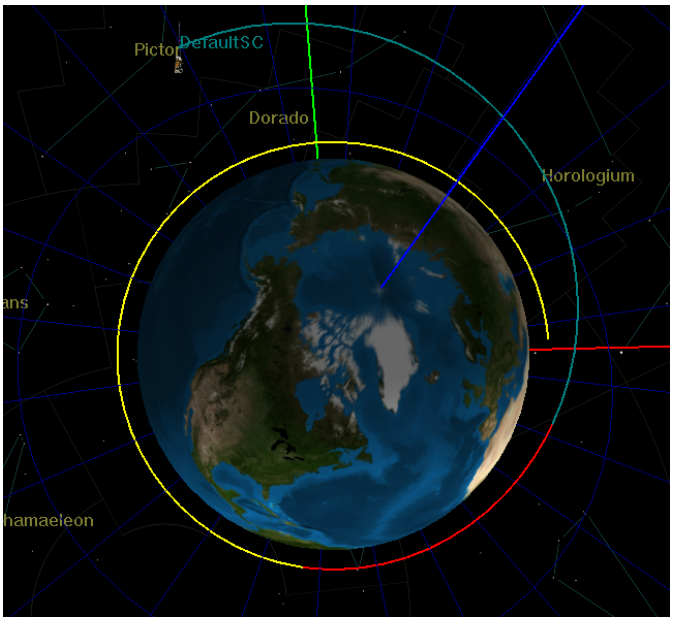

Figure 1.1: Apogee raising maneuver with GMAT software [5]. The yellow line is the initial orbit with an orbital period of approximately 1h:40m, the red line is the finite burn trajectory which takes about 20 m and the fade blue line is the state propagation until the new apoapsis

- The current orbit is constantly changing and the maneuver has to take that into account and it can be difficult, impossible, or undesirable to reach the exact planned final orbit obtained with the impulsive approximation (explained bellow).

Initial thrust to weight ratios (T/W_0) also influence the finite burn losses. Lower thrust to weight ratios lead to longer maneuvers and therefore higher finite burn losses and cases below a ratio of T/W_0=0.5 should be subject to further study [4].

How each of these factors influence the final result of a delta-v produced versus the estimated is crucial to estimate accurately the performance of the real maneuver.

Gravity loss is a phenomenon first suggested by Herman Oberth and it is sometimes referred as the Oberth's effect [6]. It is the recognition that, in the presence of a gravitational well, the same amount of propellant on a spacecraft can have different energetic outcomes for the spacecraft final motion. The burn's efficiency is larger if the spacecraft is at lower gravity potential points of its orbit, ideally the periapsis, because propellant is expelled with lower potential energy and higher kinetic energy .

Steering losses derive from the geometrical difference between the impulsive approximation and the actual finite burn trajectory and thrust direction. Although an optimal thrust direction can be computed, we also have to consider the feasibility of such optimal steering for the spacecraft system in question. In practice, the steering may have constraints. This work considers the three cases of optimal maneuvers with the constraints of: constant thrust direction; constant angular rate (as done in Cassini insertion maneuver [7] and upper stages), that covers most relevant cases, and thrust aligned with the velocity.

Regarding the instantaneous orbital change, since the maneuver is made through an arc and not a point, reaching the planned maneuver becomes a problem of reaching all 6 orbital elements of the final orbit. What generally happens is that, in this level of guidance, targets are defined which are different for

each mission. For example, it can be an escape velocity and the direction in space or in the Hohmann transfer presented an apogee. This implies that we are not comparing the finite burn maneuver to an equivalent impulsive maneuver but to one that achieves some objectives in the best possible way (optimized).

Burn losses can then be defined as the difference between the ideal impulsive maneuver and the real finite one, optimized taking the constraints into account.

1.3 Literature review

The real finite burn maneuvers can be determined numerically or analytically with an optimization method that can be direct or indirect.

In [8] it is theorized the modelling, design and optimization of finite burn maneuvers for a generalized trajectory. The issues associated with controlled engine burn maneuvers of finite thrust magnitude and duration are presented in the context of designing and optimization for a wide class of finite thrust trajectories. Although the link between a theoretical optimal thrust solution and its feasibility is debatable, as it depends on each specific spacecraft system design, this state of the art optimization method can be considered the optimal numerical solution for a finite-burn maneuver. It has been implemented in Copernicus [9], a trajectory design and optimization system, that unfortunately is not available to the wide public.

On the other hand, an open source software GMAT [5], General Mission Analysis Tool, developed by NASA, private industry, public, and private contributors can be used to simulate the environment. However the results are subject to the tool available for numerical and optimization methods (shooting methods) and to the weak costumer support it has. Nevertheless, some representative results can be obtained using this software and can be used for code validation.

A Matlab script of optimal Finite-burn for interplanetary injection from Earth orbit [10] is used as the basis for the tool computing the finite burns. The original script uses SNOPT optimizer [11] to compute optimal thrust angles for given segments of the burn via direct shooting. The modified version, uses different settings of thrust and different optimization constraints.

Analytic approaches can be used, but most studies determine a trajectory under some assumptions that limit the application of the final expressions, which make them unhelpful for this work.

For example, in [12] expressions that describe the trajectory of a high thrust maneuver are presented under the assumption that the thrust's direction is normal to the focal radius of the trajectory and the focal radius' change is small during the thrusting time interval. The expressions obtained are hardly useful for gravity loss analysis as the radial distance variation is considered to be small and the steering policy is adequate for thrust parallel to the LVLH frame, but nor for the types of maneuvers considered in this work.

Finite-thrust escape and capture trajectories are considered from either circular or elliptic orbit and the efficiency are determined in [13]. The efficiency penalty due to finite-thrust is solved by applying a correction factor to the impulsive velocity increment. It considers tangential steering (thrust vector paral-

lel to the velocity vector) and numerically integrates the maneuvers. The results are shown graphically for a wide range of jet velocity values and initial dimensionless acceleration and can then be used to apply to any particular similar case of interest — a specific planet, parking orbit, propulsion system and hyperbolic velocity. It is also shown that the difference between tangential steering and optimal steering is negligible. Nevertheless, as mentioned earlier, the specific constraints of the system are not always compatible with tangential steering, and this type of maneuver is not always optimal.

An intuitive analysis on the finite burn losses in which an analytic formula is determined for computing the losses is done in [14]. It considers that the finite thrust steering is of constant angular motion. It can be used for a general impulsive maneuver as long as the burn time is short enough. It must be mentioned that the expression needs numerical experimentation, which has not been found in the literature.

Chapter 2

High thrust maneuvering

In this chapter, we will describe how maneuvers can be determined analytically and numerically and how spacecrafts perform them.

2.1 Problem definition

Real maneuvers take some time and while the burn is occurring the spacecraft goes through different instant Keplerian orbits. As a result, it is non trivial to reach the exact orbit equal to the one from an instantaneous approximation. Generally the real maneuver is not planned to obtain exactly the instantaneous orbit but instead to accomplish certain objectives, such as the simple cases of reaching an apogee or energy level. This raises the question of how accurately the finite burn losses of the finite maneuver can be compared to the instantaneous approximation. In this work maneuvers in which either the apogee or the asymptotic velocity V_∞ are the same on both maneuvers are considered.

To solve the maneuver problem variables such as burn duration and thrust direction need to be determined so that the objectives are accomplished. At the same time it is important that the Δv is minimized, thus an optimization method must be used.

The equations of motion that describe a thrusting arc on the main body inertial frame are [15]:

$$\dot{r_x}(t) = v_x(t), \tag{2.1}$$

$$\dot{r_y}(t) = v_y(t), \tag{2.2}$$

$$\dot{r_z}(t) = v_z(t), \tag{2.3}$$

$$\dot{v_x}(t) = -\frac{\mu}{r(t)^3} r_x(t) + \frac{T_x(t)}{m(t)}, \tag{2.4}$$

$$\dot{v_y}(t) = -\frac{\mu}{r(t)^3} r_y(t) + \frac{T_y(t)}{m(t)}, \tag{2.5}$$

$$\dot{v_z}(t) = -\frac{\mu}{r(t)^3} r_z(t) + \frac{T_z(t)}{m(t)}, \tag{2.6}$$

$$\dot{m}(t) = \frac{T}{g_0 Isp}, \tag{2.7}$$

where r is the radius to the main body, v is the velocity, μ is the standard gravitational parameter, $r_x,\ r_y,\ r_z,\ v_x,\ v_y,\ v_z,\ T_x,\ T_y,\ T_z$ are the radius, velocity and Thrust in the inertial axes, Isp is the specific impulse and g_0 is the gravity acceleration at the surface of the Earth.

The following assumptions were made:

- Thrust magnitude is constant, being similar to bi-propellant liquid engines;
- Specific impulse is constant;
- Initial and final orbit are keplerian;
- maneuvers are two-dimensional, x and y plane

Because thrust and specific impulse are considered constant throughout the burn, the mass-flow rate is constant (2.7).

We consider three steering laws (for the Thrust $T_x\ T_y\ T_z$) in this work: Inertially fixed thrust direction:

$$T_x = \cos(\alpha)T, \tag{2.8}$$

$$T_y = \sin(\alpha)T, \tag{2.9}$$

$$T_z = 0, \tag{2.10}$$

where T is the thrust magnitude.

For thrust direction resulting from a constant rate about a single inertially fixed axis we modify the angle to:

$$\alpha = \alpha_0 + \dot{\alpha}t, \tag{2.11}$$

Thrust direction aligned with the velocity:

$$T_x = \frac{v_x}{v}T, \tag{2.12}$$

$$T_y = \frac{v_y}{v}T, \tag{2.13}$$

$$T_z = 0, \tag{2.14}$$

where v is the velocity magnitude.

Considering that

$$C_3 = v_\infty^2, \tag{2.15}$$

the optimization problem can be formally defined as:

minimize	Δv
w.r.t	α_0, $\dot{\alpha}$, t
subject to	$C3_{\text{finite}} = C3_{\text{impulsive}}$ for escape or
	apogee radius$_{\text{finite}}$ = apogee radius$_{\text{impulsive}}$ for apogee raising
	steering law

In the cases considered minimizing Δv is the same as minimizing the burn duration t because the mass flow rate and specific impulse are constant.

2.1.1 Maneuver dynamics

T/W_0 and I_{sp} are important parameters in maneuvers and they define how the maneuvers can differ. As we can see the acceleration magnitude is dependent on them; recalling the mass flow rate equation (2.7):

$$\frac{a(t)}{g} = \frac{\frac{T}{W_0}}{1 - \frac{T}{W_0}\frac{1}{I_{sp}}t}, \tag{2.16}$$

The acceleration of the thrust magnitude as a function of time depends only on these two variables.

2.2 Analytic estimate and trajectories

In order to predict the Δv of a maneuver we can describe the transfer orbit with an expression. The process of determining the spacecraft motion under continuous thrust is typically as follows [16]: we define the state equations on a given frame carefully chosen and a thrust steering rule. Then we define the boundary conditions which can be: the initial orbit is circular (and it becomes easy to describe it). The integration can be left dependent on the burn time or a specific boundary end condition.

The end condition in the literature is generally a simple case and on specific reference frames, which limits the solutions to low range of applicability [16] [13] [12]. To generalise this process into other boundary end conditions we would have to describe each boundary end condition with an expression that contains the orbital elements from the state equations defined earlier. Since there are no analytic trajectories that describe the cases used in this work, trajectory expressions are not used.

On the other hand it is possible to obtain an approximation or bounds for a maneuver's Δv. In this work the analytic estimate tested is the expression obtained in [14], (2.17). The expression explicitly gives a maximum value for what the finite burn losses can be. It is determined by adding to the instantaneous velocity change (of the usual instantaneous maneuver approximation) a position displacement

compensation factor obtained from a maneuver done with thrust being applied at an arbitrary constant angular velocity.

This upper limit is

$$\text{FiniteBurnlosses} \leq \frac{1}{24}(w_s t)^2 \Delta v, \tag{2.17}$$

where

$$w_s^2 = \frac{\mu}{r^3} \tag{2.18}$$

(which is related to a maximum optimal angular rotation of the thrust), t is the burn time and Δv is the instantaneous approximation velocity change. The burn time must be computed previously for the specific impulse and thrust over weight.

The Tsiolkovsky rocket equation [17]:

$$m_p = m_i \left(1 - e^{\frac{-\Delta v}{Isp g_0}}\right), \tag{2.19}$$

where m_p is the propellant mass spent on a maneuver with a certain Δv, m_i is the initial mass, Isp is the specific impulse and g_0 is the gravitational acceleration at the surface of Earth. Knowing the mass flow rate (2.7), which is constant as a result of the thrust and specific impulse being considered constant in this work, we can determine the time it would take to spend that mass:

$$t = \frac{g_0 I_{sp} m_p}{T} = \frac{I_{sp}\left(1 - e^{\frac{-\Delta v}{Isp g_0}}\right)}{\frac{T}{W_0}}, \tag{2.20}$$

where W_0 is the probe weight, and T is the thrust magnitude, related by

$$\frac{T}{W_0} = \frac{T}{g_0 m_i}, \tag{2.21}$$

2.3 Numerical determination of high thrust maneuvers

The keplerian orbit is described by the 6 classical orbit elements which can be determined by the position and velocity at a given point in time. The instantaneous approximation is just the difference of the final minus the initial velocities, whereas in the real finite maneuver it becomes a problem of optimization or targeting. The parameters involved, such as the burn time and direction, are obtained to meet the constraints.

2.3.1 Optimization methods

Trajectory optimisation methods can be either direct or indirect. In the next paragraphs we will follow [18].

Indirect methods are based on a variational calculus principle: the Pontryagin minimum principle. It is possible to formulate a two-point boundary problem with a set of adjoint variables and a switch function, the solution of which will yield a history of the time-dependent controls, the so called Hamiltonian system.

Direct methods differ from the indirect in that the time-dependent controls are described by a finite set of parameters. The effect of such a limitation on the optimal solution in most problems is negligible. In this thesis the direct method single shooting is used since it is simpler and there is available in literature a script that uses it [10].

The so called single shooting is conceptually the simplest method [18]. The initial state vector values are specified and the trajectory is progagated forward in time, with the control variable values obtained from the parameterised representation. At the end of the propagation, some of the required constraints may be met and others not.

This work uses SNOPT [11] and YUKON (from GMAT [5]) as optimization algorithms for the non-linear programing problem. Both use sequential quadratic programming which is an iterative procedure that models the non-linear problem by iteration with quadratic programming sub problems (where the objective function is a quadratic function arranged with information obtained from the differentiation of the problem, the gradient and the Hessian) [19].

Two types of constraint can be applied to the trajectory:

- functions of the state and control variables over regions of the trajectory
- functions of the state and controls at the end of the trajectory or at a fixed event

Regarding the control variables, such as the burn duration, the initial angle of the Thrust or the rotation, they are constrained within certain values. For terminal conditions we can generally use the characteristic energy C_3 for an interplanetary insertion maneuver, or a certain apogee for an orbiting satellite. Some constraints and their relation to the orbital elements on an onboard guidance algorithm of the Inertial Upper Stage Rocket are shown in table 2.1.

Table 2.1: Orbital element constraints relationships shown in [20]. γ is the flight path angle, h is the angular momentum and C_3 is the characteristic energy, R is the magnitude of the radial distance vector, V is the magnitude of the velocity vector.

Constraint elements	Equivalent constraint	
C_3 or R and V for a circular orbit	a	Semimajor axis
h and C_3 or R,V and γ for a circular orbit	e	Eccentricity
h and h_z or $\vec{h}$ for (i=0)	i	Inclination
h, h_z, e_z and C_3	ω	Argument of perigee
h_x and h_y	Ω	Right ascension of ascending node

The characteristic energy is defined as

$$C_3 = v_\infty^2 \tag{2.22}$$

where V_∞^2 is the asymptotic velocity at infinite distance of an hyperbolic keplerian orbit.

In this work some of the constraints are not used such as the inclination or direction of an hyperbola, these can be considered to be accomplished by the booster and time of launch. For the case of escape maneuver we use the characteristic energy C_3, which is equivalent to the asymptotic velocity (2.22). For a Hohmann transfer to higher orbit we use the apogee, applicable for general orbiting probes, interplanetary orbiters (when reaching a planet) or some geostationary satellites.

2.4 Typical approaches to real maneuvers

Information about real maneuvers is scarce in literature but there are a few examples. Generally, upper stages perform maneuvers with constant thrust direction or constant rotation probably because their mass and size makes it difficult to control the attitude, whereas satellite maneuvering is more flexible since they are smaller and can be more maneuverable.

In Mars Observer mission [21], the orbit insertion by the upper stage was planned to start burning at a defined radius with constant flight path angle. Such strategy simplified the system guidance software. Meanwhile, the satellite performed all maneuvers by pitching at a constant rate about an inertial fixed axis.

In the Apollo missions in the Trans-Lunar Insertion performed by the upper stage is suggested to have been done in constant pitch direction in [22].

In the Mars Global Surveyer mission the spacecraft used a ”pitch-over” steering strategy for the Mars orbit insertion in order to maximize the efficiency of the burn. ”Pitch-over” works by using the attitude control thrusters to slew the spacecraft at a constant rate during the 20 minute to 25 minute burn in an attempt to keep the thrust tangent to the trajectory arc [23].

Considering the above practical examples, the choice of the three steering cases are within the real maneuvers.

2.4.1 Typical spacecraft systems

In the table 2.2 some important parameters are shown for different types of spacecraft.

Table 2.2: Propulsion and payload values parameters for different types of missions

Spacecraft	Thrust, N	Isp, s	Mass, kg	T/W_0	Utility	ref
Fregat	19 850	332	7 538	0.2687	Upper stage	[2]
Centaur	99 200	450	23 073	0.4387	Upper stage	[3]
Venus express orbiter	414	317	1 245	0.0339	Interplanetary satellite	[24]
Mars Global Surveyur	596	318	1 052	0.0582	Interplanetary satellite	[25]
Cassini	440	305	5 574	0.0080	Interplanetary satellite	[26]
INSAT-3D	440	Na	2 120	0.0212	Geostationary satellite	[27]

For apogee maneuvers in Geostationary satellites generally the engines have typically 490 N of thrust and 310 Isp [28].

Considering the above examples of spacecrafts, for this work we used a range for T/W_0 of 0.03 to 0.5, for specific impulse of 300s, 400s, and 600s.

2.4.2 Multiple apogee raising maneuver

We can use the technique of apogee raising to minimize the burn losses. By dividing the direct Δv in smaller ones, each burn will be shorter and closer to the main body, taking advantage of the Oberth effect. Whereas a direct maneuver would last longer and the burn would take place in a trajectory that would eventually be further away from the main body. Thus multiple apogee raising maneuvers save Δv and have a significant impact on mission planning such as in the mission chandrayaan-2 [29].

2.5 Cases studied

In this work the maneuvers determined start from a circular parking orbit of 200 km altitude, with ideal Δv ranging from 1 km/s to 5 km/s with a step of 0.5 km/s, for T/W_0 from 0.03 to 0.5 with a step of 0.01 for a specific impulse of 250 s, 300 s, 400 s and 600 s for the three steering laws.

Then as an alternative to direct maneuvers, the multiple apogee raising maneuver is studied for a specific impulse of 300 s and $T/W_0 = 0.15$ for a transfer orbit to Mars and for a geostationary transfer

orbit (GTO).

Chapter 3

Numerical implementation of the direct shooting

In this chapter the details and process of computing the maneuvers numerically are presented. Two types of algorithms were developed in this work, one that determines single maneuvers (developed in MATLAB) and other that computes multiple maneuvers (developed in GMAT and MATLAB).

3.1 Single maneuver and multiple maneuvers

For both single and multiple maneuvers we used only the direct shooting method. In single maneuvers, since more than one steering law is studied it was developed in MATLAB, because it allows for more flexibility in programming the steering mechanisms. For multiple maneuvers, for the case where thrust is parallel to the velocity it was developed in GMAT because of its simplicity of implementation, whereas for the other steering laws it was implemented in MATLAB.

3.2 Single maneuver: Algorithms implemented

To determine the optimum single maneuver we used the optimization parameters:

- Thrust duration
- Initial inertial angle for thrust direction
- Inertial rotation of the thrust direction

The inputs are: the orbital elements of the initial orbit, the type of steering law and the spacecraft parameters (initial mass, specific impulse and the desired T/W_0 which then determines the thrust magnitude). The outputs are the final velocity, radius and mass (which are then converted to orbital elements), the optimal steering variables and the burn duration.

The algorithm takes the initial guesses for the optimization variables and integrates the equations of motion of the thrusting arc and returns the final values of the constraints (apogee or C3) and the objective function (which is the minimization variable, burn duration) to the optimizer. By iteration it attempts to obtain the optimal values that met the constraints. Figure 3.1 roughly illustrates the structure of the program.

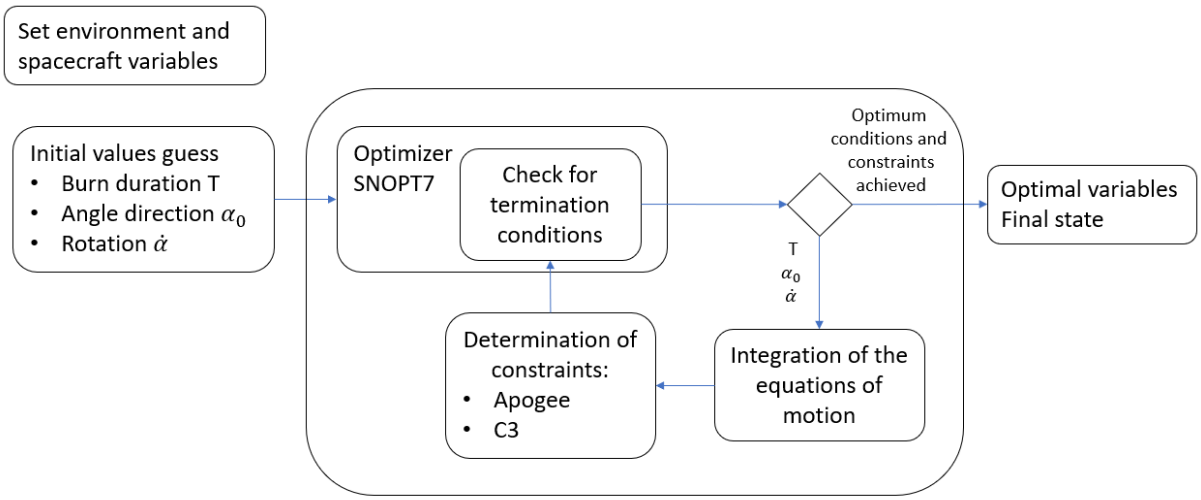

Figure 3.1: Structure of the program

The program is composed by: an optimizer, functions that apply the equations of motion, a propagator, a function that initiates the maneuver and provides the constraints and objective function to the optimizer, and functions that convert velocity and position to the orbital elements and vice-versa.

3.2.1 Propagator

The integration of the equations (2.1) to (2.7) were done with ODE45 function of MATLAB, which uses explicit Dormand-Prince method of order 4.

Initially a Runge-Kutta of the 8th order was used but it proved to be too slow with insignificant improvements and so it was later changed to ODE45.

Since the angle rotation was not included as a state equation, it should be mentioned that for the case of fixed rotation, the rotation is done with a step of the order of 2 seconds for T/W_0 lower than 0.15 and 4 seconds for higher T/W_0. Lower values were not used because the optimization took too long.

3.2.2 Optimizer

The Optimization problem was solved using direct shooting with the package SNOPT.

The shooting method is very sensitive to the initial optimization variable guesses, thus various initial guess methods were tested. The final results are a mixture of optimal results obtained with from different techniques:

- using the burn duration of thrust parallel to velocity as initial guess for the other cases;

- using the results obtained from previously computed T/W_0 for the initial angle and rotation angle;

- providing the angle rotation as if it would behave as a circular orbit (using the burn duration for averaging the initial and final angle of thrust parallel to velocity);

- or a typical value for angle rotation stated in [14],

$$\dot{\alpha} = 0.5\sqrt{\frac{\mu}{r^3}}. \tag{3.1}$$

Extra attention was paid to avoid local optima by using multiple starting points.

3.3 Multiple Maneuvers

3.3.1 MATLAB algorithm

The algorithm was further enhanced to perform multiple maneuvers. It was done for the purpose of studying a mission to Mars where the spacecraft could be large and have low maneuverability, having inertial fixed thrust steering.

The algorithm was arranged by adding a new optimization variable, the true anomaly in which the new burn starts, the burn duration, the angle direction and the angle rotation for each extra maneuver. The structure is the same.

3.3.2 GMAT algorithm

GMAT is used for multiple apogee raising maneuvers with thrust aligned with velocity. The program works with objects such as a spacecraft, a thruster or a tank. Then we can associate the created thruster or tank to a spacecraft.

For example, The thrusters can be defined in several axes such as an Earth equatorial inertial axis, a LVLH (Local Vertical, Local Horizontal) frame and the one used: VNB (Velocity, Normal, Binormal, x axis aligned with the velocity). These axes define the steering law. Simply by using VNB axis, we can compute the case of thrust parallel to velocity.

We considered that the burn times of each maneuver are the variables. Starting from a circular orbit it propagates the first maneuver and then propagates to the new perigee where two variables are used: one for backward propagation defining the initial point of the new burn and the other the burn time. The boundary end constraint is the semimajor axis and it determined after the final maneuver. The semimajor axis is equivalent to the orbit's energy, and so to the asymptotic velocity. The minimization variable is the sum of the time of the maneuvers performed, which is again equivalent to minimizing Δv, since the thrust and specific impulse are modelled constant.

3.4 Code test and validation

We compared the program developed with the one offered by GMAT for various T/W_0 for the case of thrust parallel to velocity. The difference in the results was $0.001\,\%$ which we considered acceptable. The difference is probably due to larger tolerance in the GMAT optimizer when reaching the target.

Chapter 4

Results for real maneuvers

In this chapter, the finite burn losses and effects on the final orbit are determined and discussed. The three steering cases are compared to each other and to the heuristic from literature [14] and effects on the perigee are shown.

4.1 Burn losses for the three types of steering considered

We study a maneuver equivalent to an impulsive maneuver of the stated Δv. The Δv is increased from $1\,\mathrm{km/s}$ to $3\,\mathrm{km/s}$, where the orbit after the maneuver is elliptical and can be thought of as a transfer orbit of a Homann transfer. Above $3\,\mathrm{km/s}$, the resulting orbit is hyperbolic and can be thought of as an escape maneuver, resulting in a certain C3. The raise of Δv was thought to cover many interesting cases from apogee raising maneuvers to GTO transfers and escape trajectory to Mars. We study the Δv losses as a function of T/W_0 for a specific impulse of $300\,\mathrm{s}$, (but also for $250\,\mathrm{s}$, $400\,\mathrm{s}$, $600\,\mathrm{s}$) deemed a representative value for modern technology.

In this work the maneuvers determined start from a circular parking orbit of $200\,\mathrm{km}$ altitude, with ideal Δv ranging from $1\,\mathrm{km/s}$ to $5\,\mathrm{km/s}$ with a step of $0.5\,\mathrm{km/s}$, for T/W_0 from 0.03 to 0.5 with a step of 0.01 for a specific impulse of $250\,\mathrm{s}$, $300\,\mathrm{s}$, $400\,\mathrm{s}$ and $600\,\mathrm{s}$ for the three steering laws.

Then as an alternative to direct maneuvers, the multiple apogee raising maneuver is studied for a specific impulse of $300\,\mathrm{s}$ and $T/W_0 = 0.15$ for a transfer orbit to Mars and for a geostationary transfer orbit (GTO).

The finite burn losses can be defined as

$$\text{FiniteBurnLosses} = \text{Real } \Delta v - \text{Impulsive } \Delta v \tag{4.1}$$

For a specific impulse of $300\,\mathrm{s}$, figure 4.1 shows the results for thrust parallel with velocity (vnb), figure 4.2 with fixed direction (c), and figure 4.3 with inertial fixed rotation (w).

The baseline results are similar to existing literature, as seen in figure 4.4 [4], although no information about how those results were obtained is available.

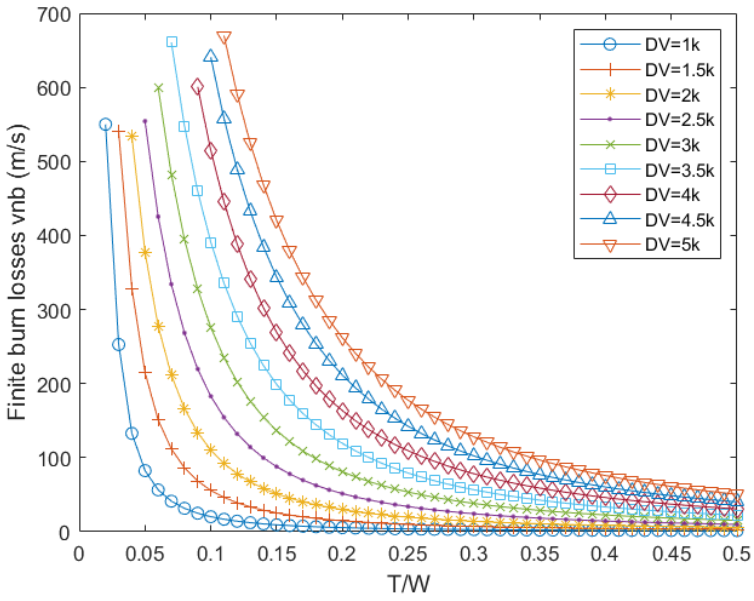

Figure 4.1: Finite burn losses with direction of the Thrust parallel to the velocity (vnb) for Isp = 300 s. Dv represents the impulsive Δv in m/s and k stands for thousand.

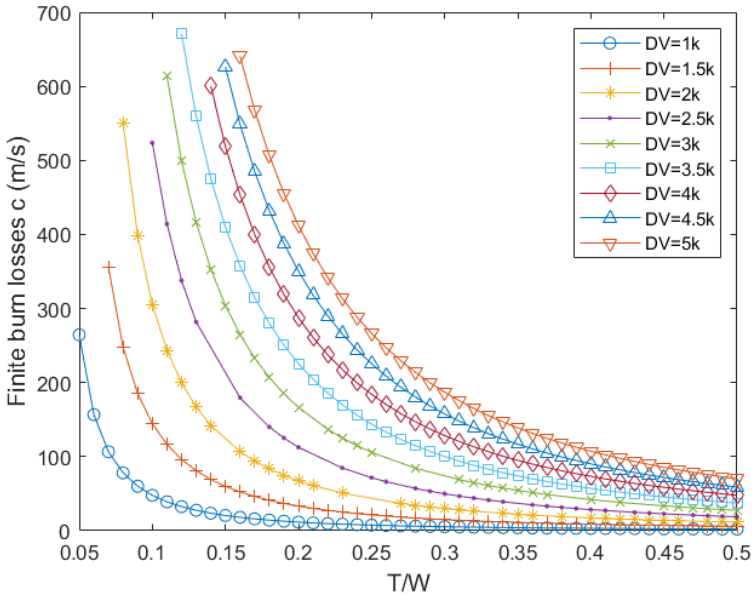

Figure 4.2: Finite burn losses with inertial fixed direction (c) of the Thrust for Isp = 300 s. Dv represents the impulsive Δv in m/s and k stands for thousand.

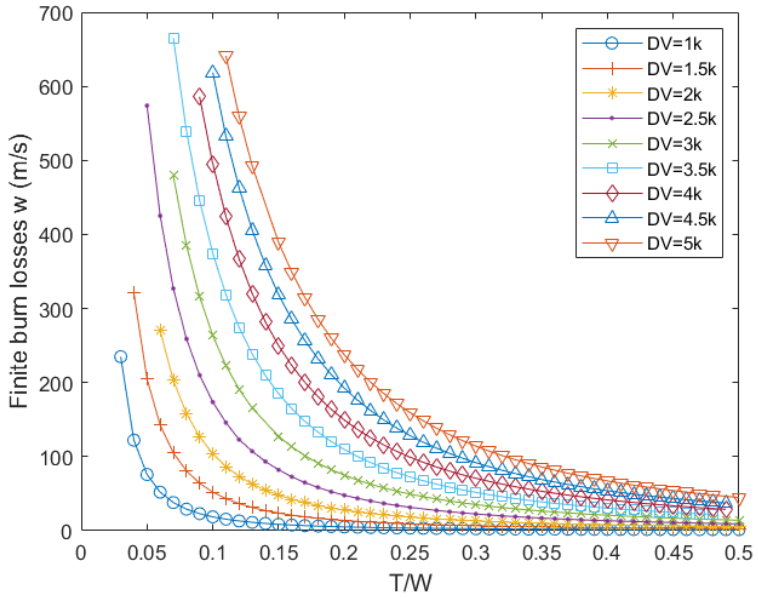

Figure 4.3: Finite burn losses with inertial fixed rotation (w) of the Thrust for Isp = 300 s. Dv represents the impulsive Δv in m/s and k stands for thousand.

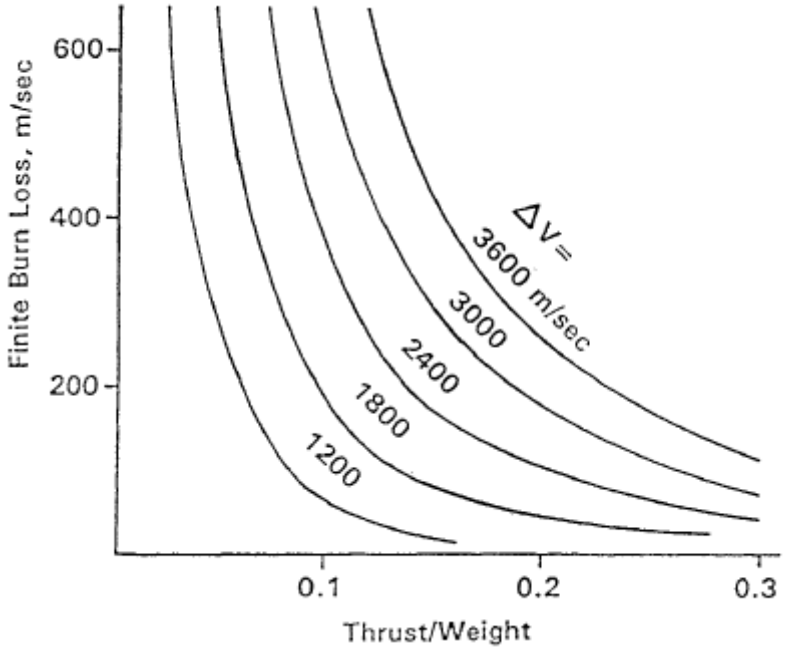

Figure 4.4: Finite burn losses from [4]

All cases present the same pattern where the finite burn losses highly increase below a certain T/W_0, whereas for higher T/W_0 the curves are quite close to each other, as the duration of the maneuver are shorter and the steering law has less effect on the losses. It can also be seen that figures 4.1 and 4.3 look similar. For $T/W_0 = 0.05$, for the lowest Δv, the finite burn losses on both cases are around 75 m/s, while on figure 4.2 they are around 250 m/s. In other words, a comparison of figures 4.1 and 4.3 shows that the difference in burn losses between the cases of Thrust parallel to velocity and thrust with

constant rotation is very small. On the other hand, the performance of thrust with constant direction is clearly worst.

For a specific impulse of 400 s figure 4.5 shows the results for thrust parallel with velocity (vnb), figure 4.6 with fixed direction, and figure 4.7 with with inertial fixed rotation.

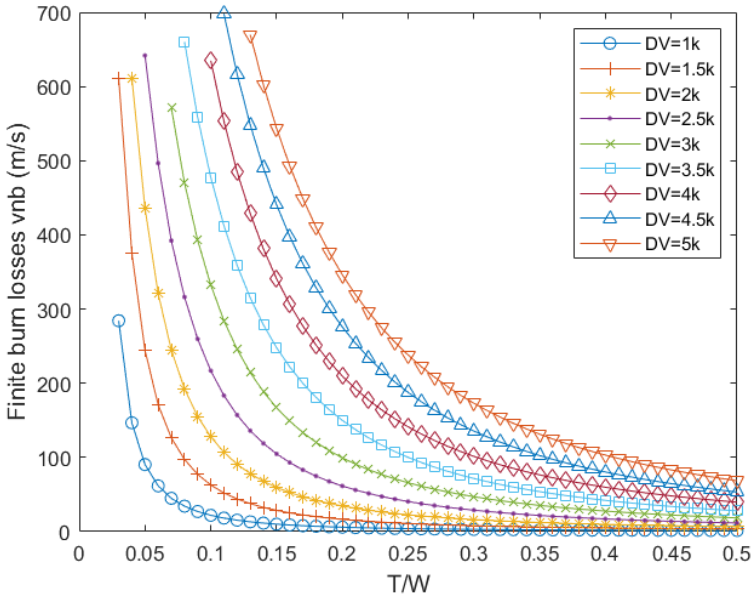

Figure 4.5: Similar to figure 4.1, we can see the finite burn losses with direction of the Thrust parallel to the velocity for Isp = 400 s

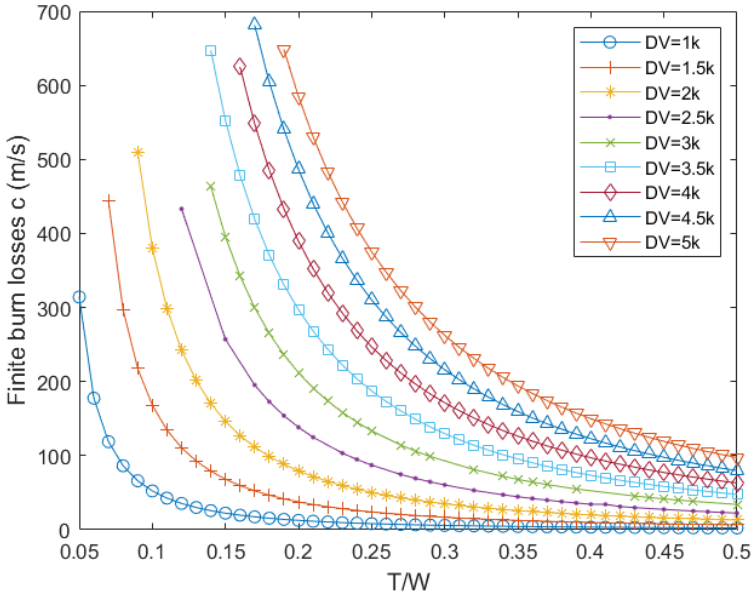

Figure 4.6: Similar to figure 4.2, we can see the finite burn losses with inertial fixed direction of the Thrust for Isp = 400 s

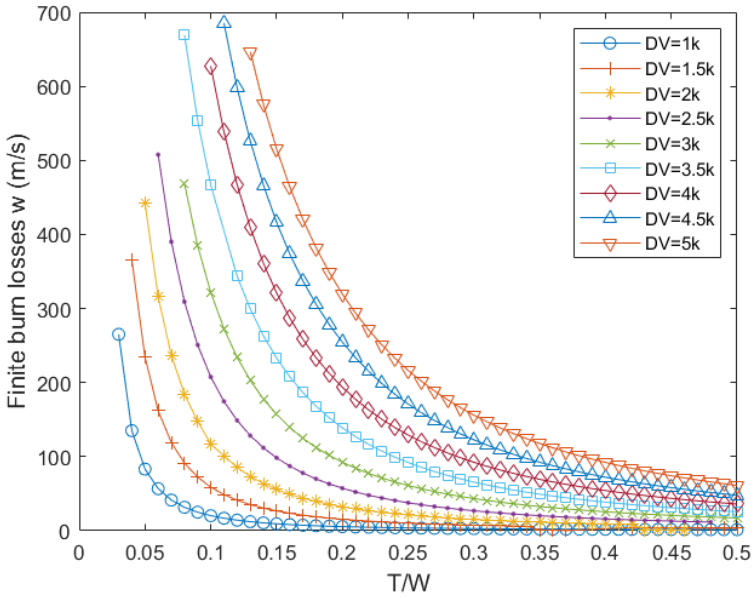

Figure 4.7: Similar to figure 4.3, we can see the finite burn losses with inertial fixed rotation of the Thrust 400 s

For a specific impulse of 600 s figure 4.8 shows the results for thrust parallel with velocity, figure 4.9 with fixed direction, and figure 4.10 with with inertial fixed rotation:

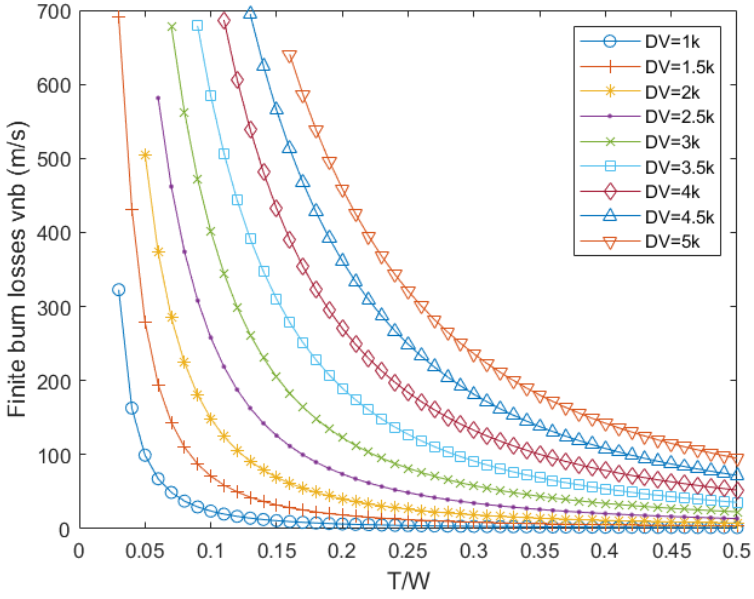

Figure 4.8: Similar to figure 4.1, we can see the finite burn losses with direction of the Thrust parallel to the velocity for Isp = 600 s

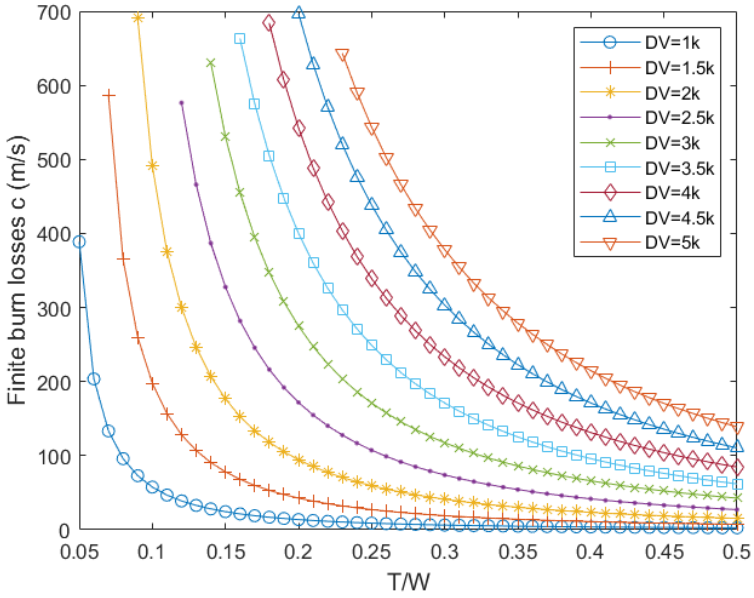

Figure 4.9: Similar to figure 4.2, we can see the finite burn losses with inertial fixed direction of the Thrust for Isp = 600 s

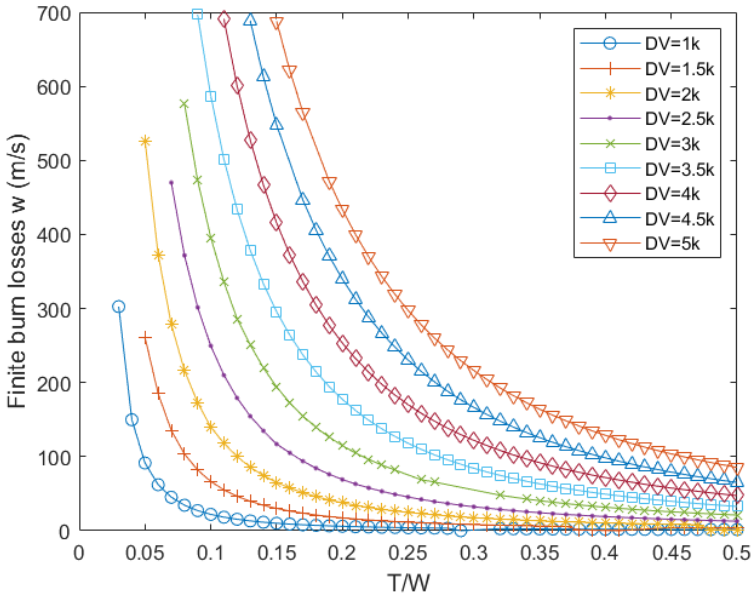

Figure 4.10: Similar to figure 4.3, we can see the finite burn losses with inertial fixed rotation of the Thrust for Isp = 600 s

4.1.1 Comparing losses with different specific impulse

We can compare the burn losses of the cases of thrust parallel to velocity between the specific impulses 400 s and 300 s. Contrary to what we could expect, the burn loss is higher for the higher specific impulse as shown in figure 4.11 (the same happens for the other steering cases).

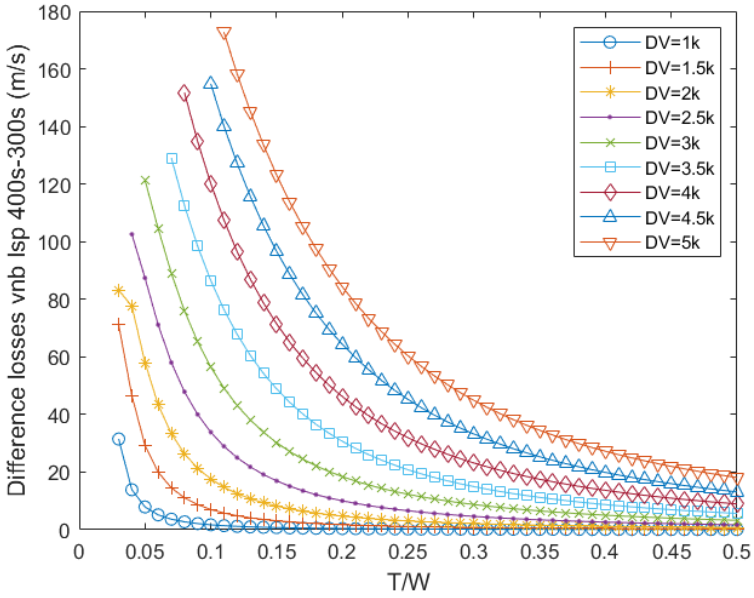

Figure 4.11: Difference of the finite burn losses between Isp = 400 s minus Isp = 300 s

This result was unexpected because intuitively it seems that a higher specific impulse should lead to lower losses. However, with a higher specific impulse, there is a lower mass flow rate for the same magnitude of Thrust. Since the acceleration increases while the spacecraft's mass decreases, if less fuel is spent, the spacecraft mass will not decrease as much and the acceleration increase rate will be lower, resulting in a longer maneuver. This is confirmed in figure 4.12 where the duration of the burn is compared between the two specific impulses and it is larger for a specific impulse of 400 s.

Despite the longer burn time, the fuel carries more energy (because of the higher specific impulse) and at the end of the maneuver, the total mass is now larger as shown in figure 4.13 where in some cases $10\,\%$ of the initial mass is saved compared to the specific impulse of 300 s. This means that the higher specific impulse maneuver is still more efficient, as it can accelerate more payload mass. That becomes clear if we start with the same dry mass in both cases, we can see those results chosen for a middle value of $T/W_0 = 0.25$ for a specific impulse of 300 s and Δv of $3.5\,\mathrm{km\,s^{-1}}$ on table 4.1, where we can see that the Δv for the same dry mass is lower for higher specific impulses.

Table 4.1: Finite burn losses for different specific impulses with the same dry mass

Isp, s	Δv, $\mathrm{m\,s^{-1}}$	new T/W0
300	3579.3	0.25
400	3556.6	0.34
600	3541.2	0.46

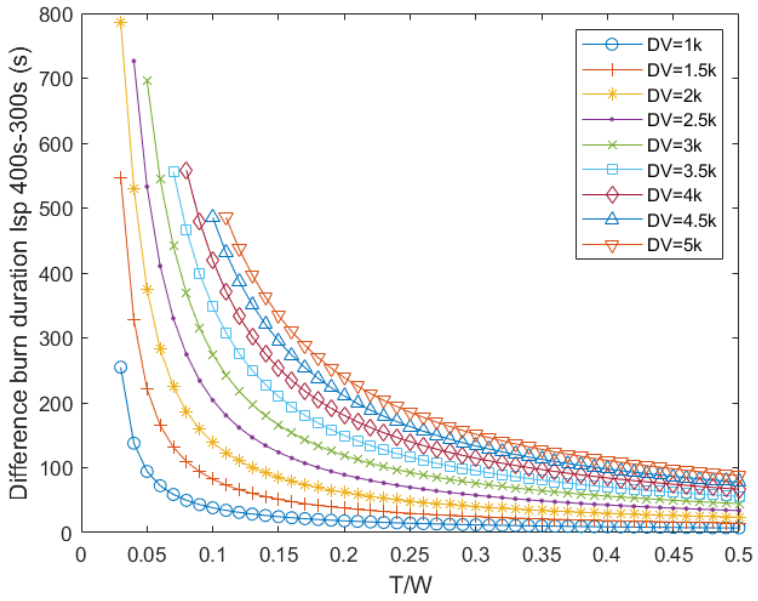

Figure 4.12: Difference of the burn duration between Isp = 400 s and Isp = 300 s

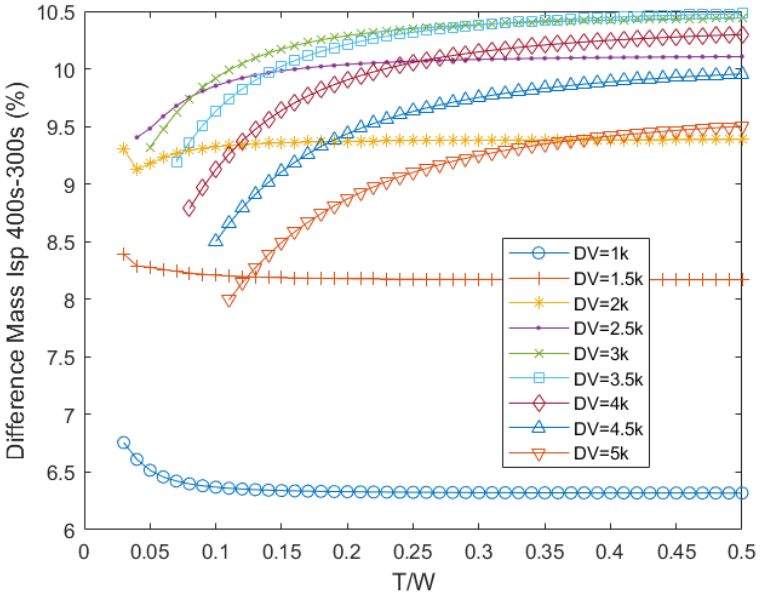

Figure 4.13: Difference of the final mass between Isp = 400 s minus Isp = 300 s in relation to the same initial mass. The change in the type of the curve corresponds to the change of the type of the final orbit after the maneuver: elliptic (apogee raising) up to Δv = 3 km/s and hyperbolic (escape) for higher Δv.

4.1.2 Comparison of the steering solutions for $Isp = 300\,\mathrm{s}$

Before analyzing the results, we would expect the thrust parallel to velocity to be one of the best performing cases, where the thrust energy is fully converted to the velocity, having the least steering losses. On the other hand, we would expect the worst performing method to be the constant thrust direction. While with rotation, it is less predictable because it is nontrivial what happens, as we will see below.

The difference between the burn losses with thrust direction parallel to velocity and constant thrust direction is shown in figure 4.14 and figure 4.15 shows the difference between constant direction and rotation. We can see that inertial fixed thrust direction is outperformed by the other steering options specially for lower T/W_0 ratios where the burn is longer, the velocity direction throughout the burn undergoes bigger changes and the misalignment between velocity and thrust is large. The higher the T/W_0 ratios (above 0.3), the smaller the difference (reaching values around $0.5\,\%$ of the impulsive approximation). Figure 4.16 shows the comparison of the cases of thrust parallel to the velocity and thrust with fixed rotation. We can see a surprising result, where the rotation case performs slightly better above T/W_0 =0.1 but for lower ratios that have higher Δv, thrust parallel to the velocity has lower losses. In general, both are very close to each other as the difference is lower than $1\,\%$ of the impulsive approximation, except around T/W_0 =0.05 where it is approximately $2\,\%$.

This is an important observation because simulating a maneuver with thrust parallel to velocity is easier than using constant rotation. Since both are similar on certain ranges we may estimate the burn losses on preliminary design stages with thrust parallel to velocity.

We can observe with more detail the comparison of these two cases by viewing the orbits of $T/W_0 = 0.15$, figure 4.17, and $T/W_0 = 0.05$, figure 4.18, for a $\Delta v = 4.5\,\mathrm{km/s}$. An interesting effect occurs where the case with rotation starts pointing slightly to inside the orbit and stays closer to the Earth throughout the orbit and takes better advantage of the Oberth effect even though the thrust isn't aligned with the velocity (in which case there is no loss of energy to the velocity due to misalignment of the thrust and velocity vectors). The thrust vector starts by pointing slightly to the main body and ends up being aligned with the velocity, achieving both proximity to the main body and effectiveness in steering.

For the $T/W_0 = 0.05$ where the rotation performs worst the results from figure 4.18 suggests that it is a long maneuver, more than half an orbit. One hypothesis of why it is worse is because now the steering effects overcome the Oberth effect gained from being closer to the main body. Nevertheless, this case is not very realistic because a maneuver taking half a period is not usually performed.

On another note, these results contradict a conclusion in [13] where it is stated that the difference of the burn losses between thrust aligned with velocity and an optimal solution is negligible, which may not be. Especially because the case of rotation is only a constrained sub-optimal case and not the optimal one.

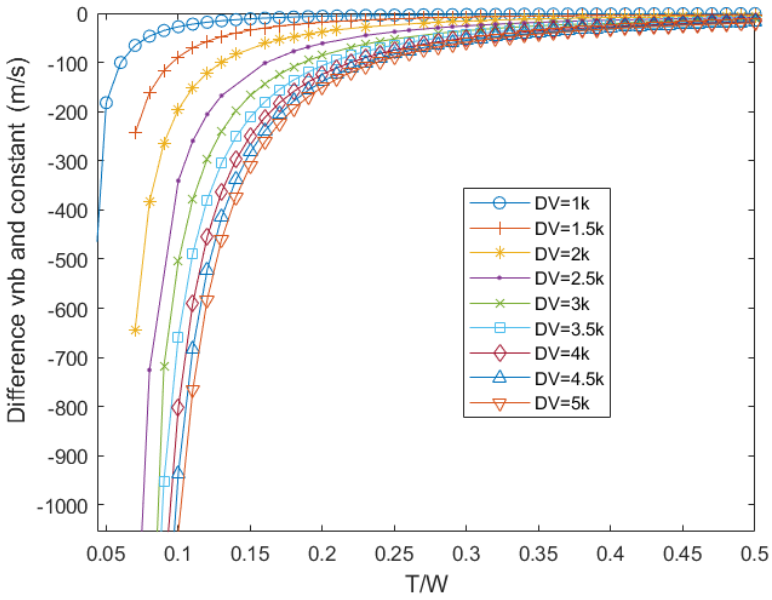

Figure 4.14: Difference between finite burn losses with direction of the Thrust parallel to the velocity and constant direction of Thrust

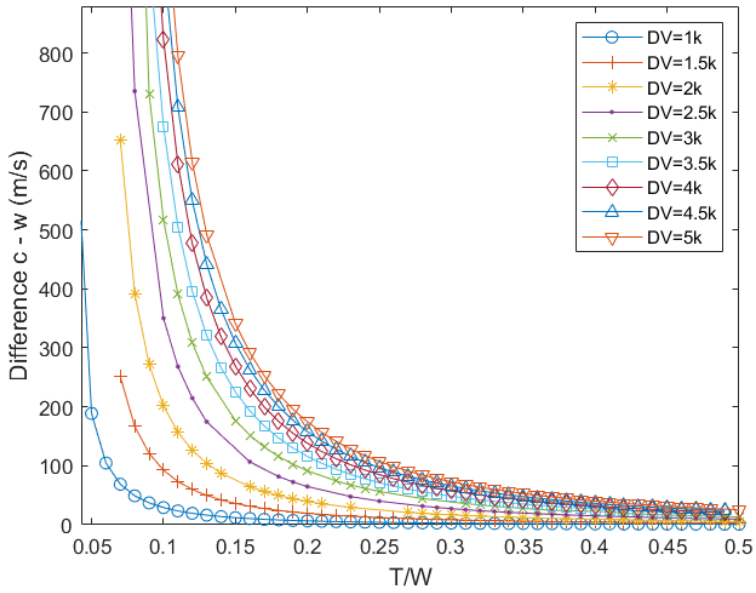

Figure 4.15: Difference between finite burn losses with constant direction of Thrust and inertial fixed rotation of the Thrust

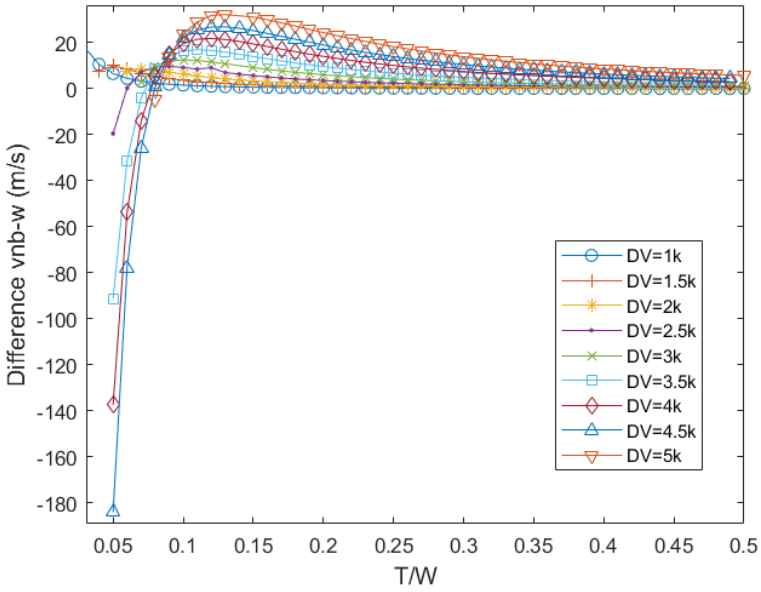

Figure 4.16: Difference between finite burn losses with direction of the Thrust parallel to the velocity and and inertial fixed rotation of the Thrust

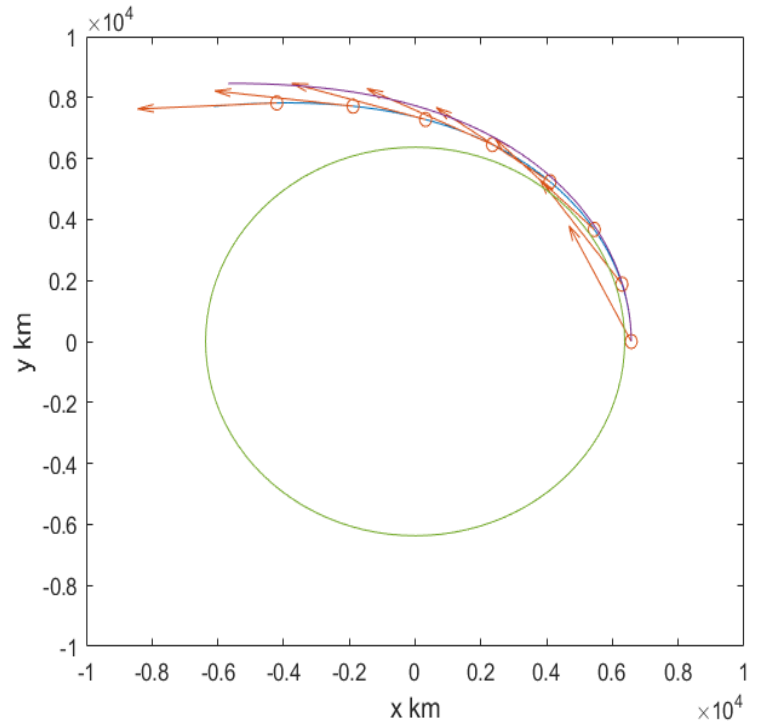

Figure 4.17: Orbits with angular rotation (the one with arrows that show the thrust direction) and with thrust aligned with velocity. The green circle represents the Earth.

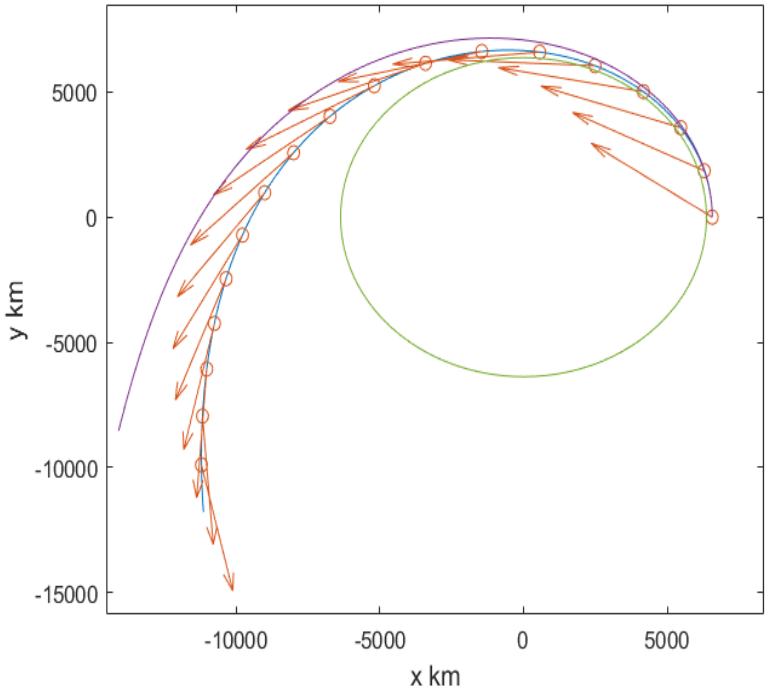

Figure 4.18: Orbits with angular rotation (the one with arrows that show the thrust direction) and with thrust aligned with velocity. The green circle represents the Earth.

4.1.3 Effects of finite burn on the perigee

By targeting only the apogee, we are not able to obtain the transfer orbit obtained in the impulsive approximation. The perigee will be different, both the value and the argument of the perigee. So it is important to analyze what happens to the variables describing the real orbit, such as the new perigee (in altitude), the velocity at the apoapsis, and the argument of the perigee.

Figures 4.21, 4.19, and 4.20 show the perigee after the burn for each steering mechanism. We can see that for the case of constant thrust, for higher T/W_0 (above 0.2) the dislocation of the perigee is small being around 1 to 10 km. For the cases of thrust rotation and parallel to velocity the perigee always increases, resulting in higher energy orbits since the apogee is the same for all the maneuvers so a higher perigee means a larger semi-major axis. On the other hand, if the thrust direction is constant the final perigee is lower; less energy was put into the orbit. This is confirmed by analyzing the results from figures 4.22, 4.23, and 4.24 which show the impulsive approximation Δv necessary for circularization at the apogee for each steering mechanism. For the constant direction case it is higher for lower T/W_0, and for the other steering cases it is lower.

Higher Δv have lower values of circularization Δv because the transfer orbit has higher energy and reaches the apogee with higher velocity. The Δv for circularization starts to decrease after a certain initial transfer orbit Δv. Figure 4.25 shows the result of an impulsive approximation Hohmann transfer where it is shown that after a certain Δv at the perigee, the circularization Δv starts to decrease.

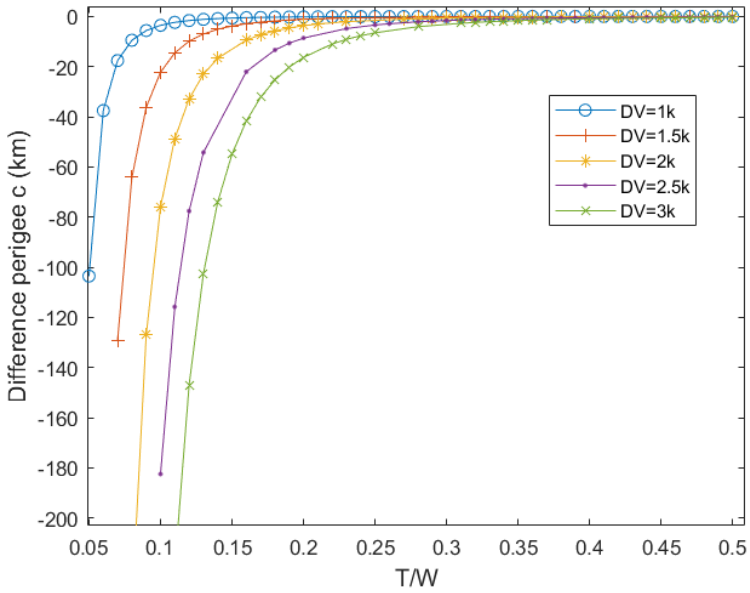

Figure 4.19: Perigee after burn for inertial constant thrust direction for specific impulse of 300 s

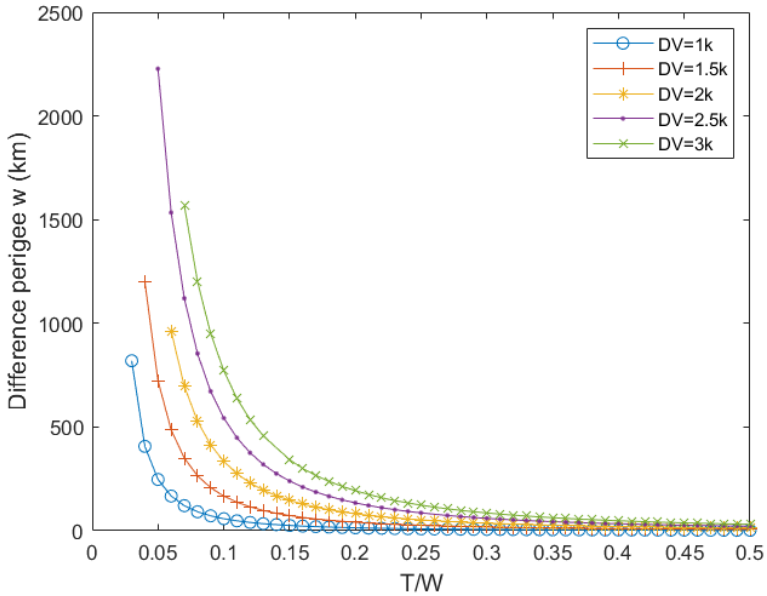

Figure 4.20: Perigee after burn for inertial constant rotation thrust direction for specific impulse of 300 s

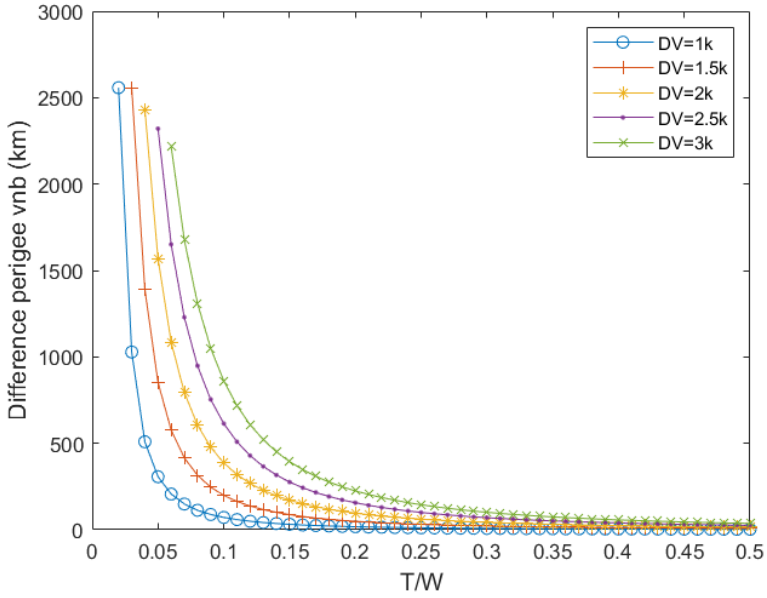

Figure 4.21: Perigee after burn for thrust direction paralel to velocity for specific impulse of 300 s

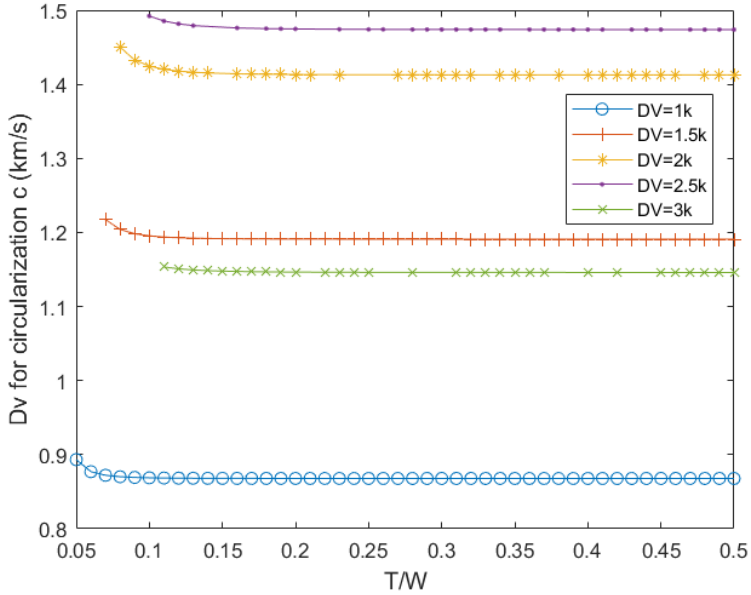

Figure 4.22: Impulsive Δv for circularization at the apogee of the orbit resulting from the initial maneuver for inertial constant thrust direction

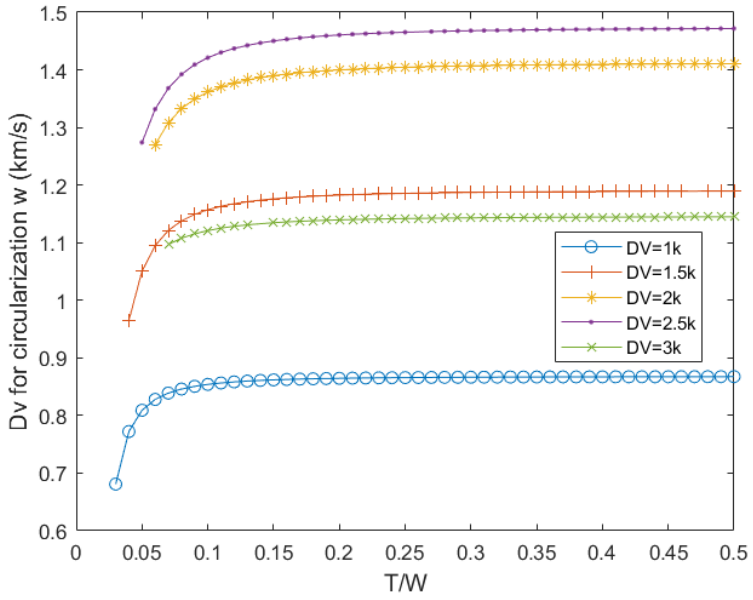

Figure 4.23: Impulsive Δv for circularization at the apogee of the orbit resulting from the initial maneuver for inertial constant rotation thrust direction

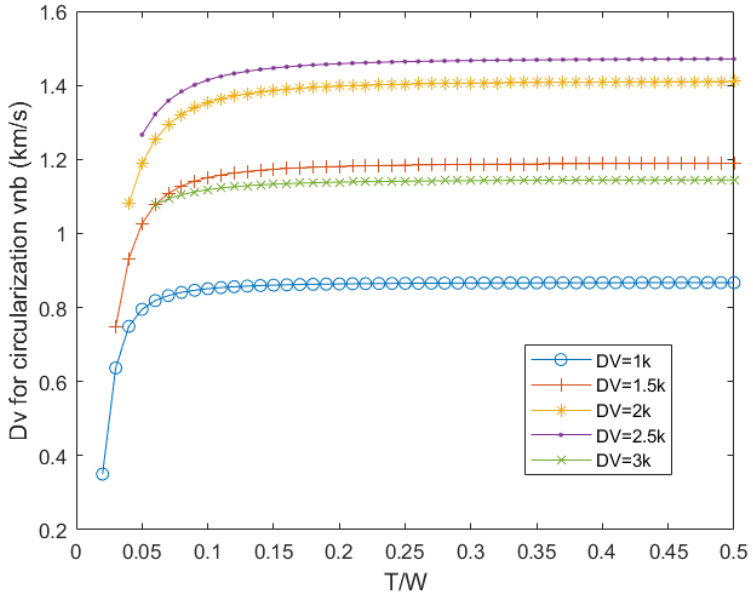

Figure 4.24: Impulsive Δv for circularization at the apogee of the orbit resulting from the initial maneuver for thrust direction paralel to velocity

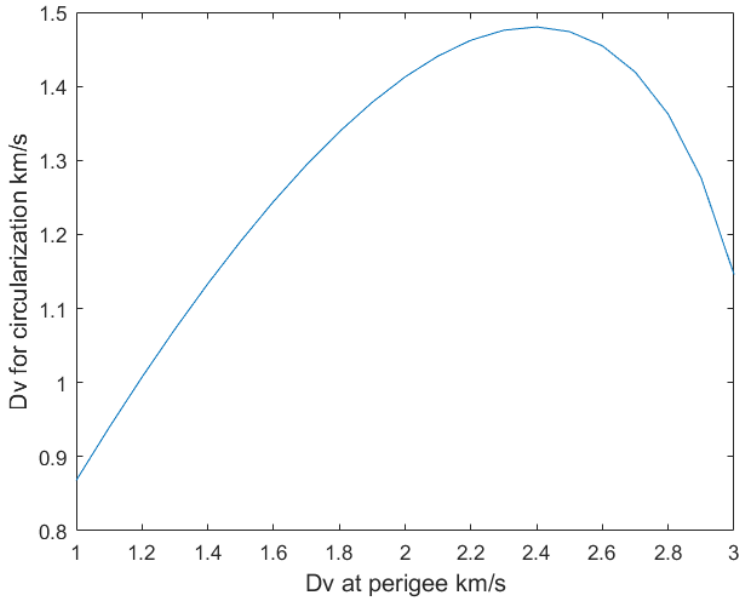

Figure 4.25: Impulsive Δv for circularization at the apogee for impulsive Hohmann transfer

The argument of the perigee also gets displaced differently between the steering cases. For both cases of thrust parallel to velocity and constant rotation the argument displacement has close values whereas for the constant direction case, its displacement is bigger, for a $T/W_0 = 0.1$ on the first two cases its around $25°$ while for the constant direction is around $35°$. It is also important to note that we start from a circular orbit (which does not have perigee), so displacements of this order are to be expected; on an elliptical orbit the burn starts before the perigee and does not result in huge changes as seen on a circular orbit (as will be seen in the next chapter, on figure 5.2 where the argument of the perigee remains close on multiple maneuvers).

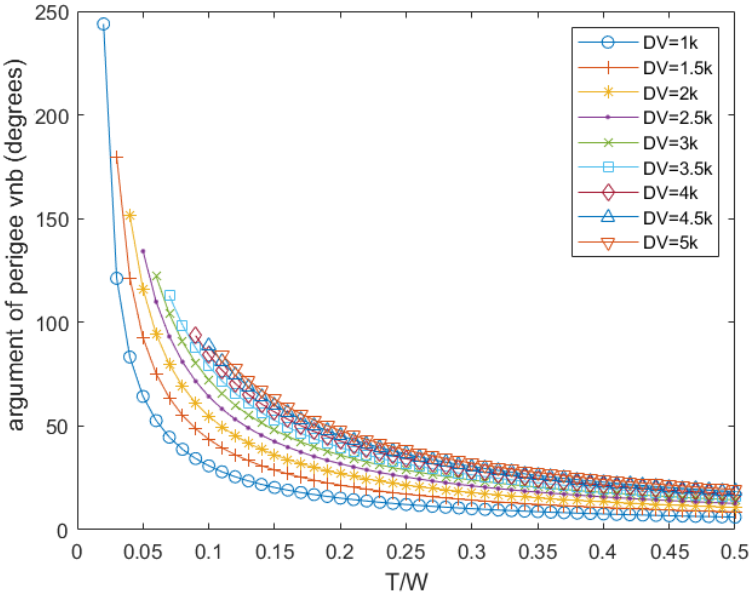

Figure 4.26: Argument of perigee for thrust parallel to velocity for specific impulse of 300 s

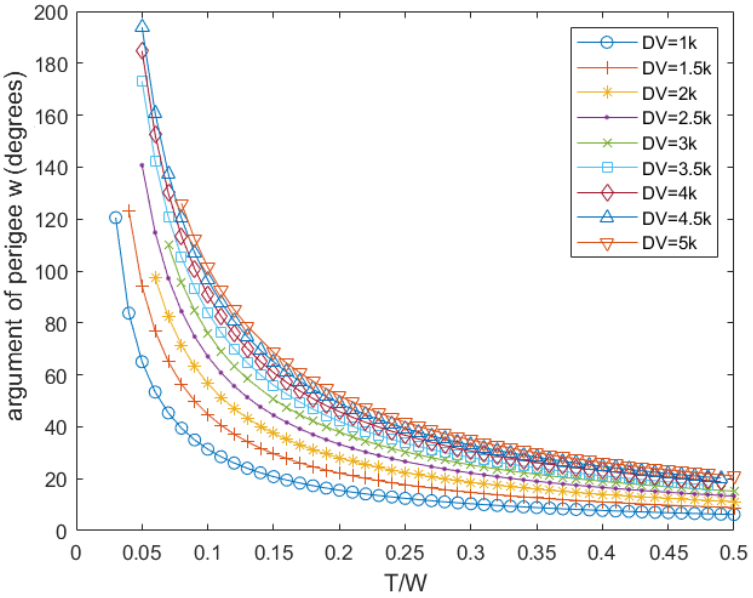

Figure 4.27: Argument of perigee for thrust with constant rotation for specific impulse of 300 s

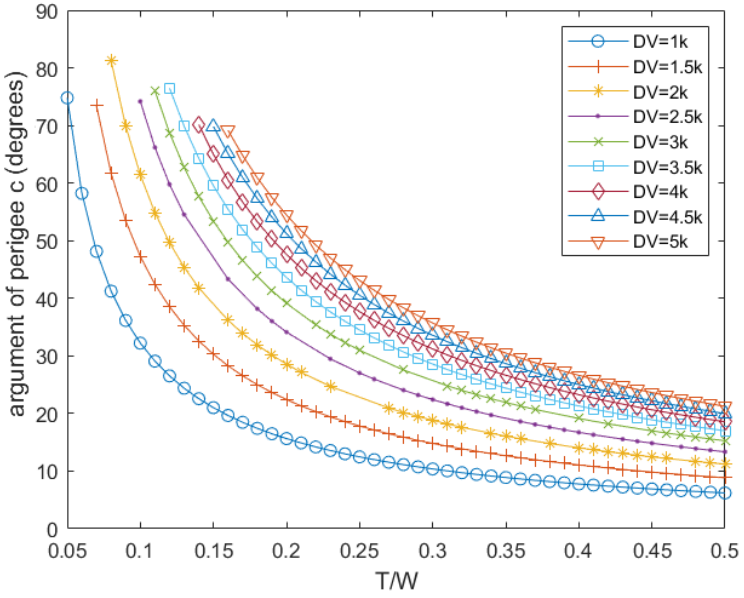

Figure 4.28: Argument of perigee for thrust constant direction for specific impulse of 300 s

4.1.4 Robustness of analytic estimate

In the figure 4.29 the finite burn losses as foreseen by the solution developed from [14] and explained in chapter 2 is presented for a specific impulse of 300 s.

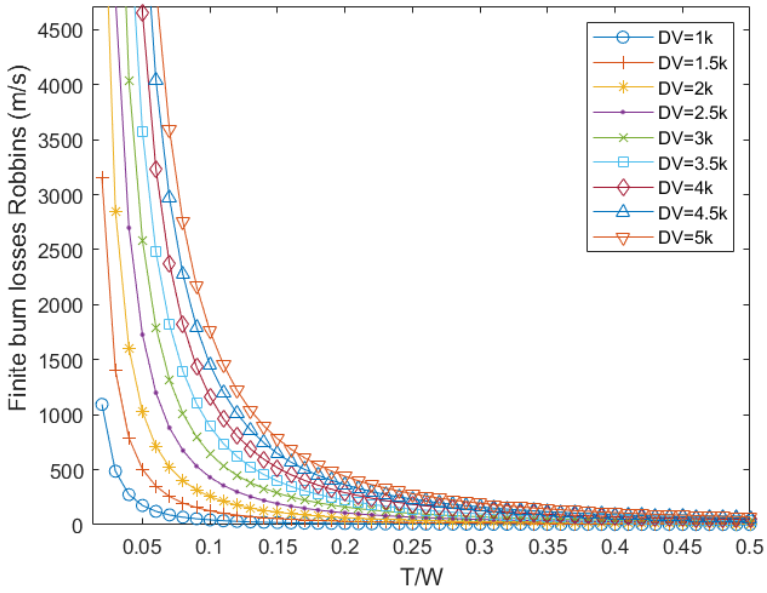

Figure 4.29: Finite burn losses from [14] for a specific impulse of 300 s

In figures 4.30, 4.31, and 4.32 it is shown the difference between the solution developed and the real case for specific impulse of 300 s. The burn losses curves are similar as observed in the real case, except for the case of constant direction where the losses are only predicted above T/W_0 0.1 for Δv higher than $3.5\,\mathrm{km/s}$. We can compare the percentage of the losses from the estimation (figure 4.29) with the real losses (figures 4.1, 4.2, and 4.3) using the relative difference of losses (4.2).

$$\text{RelativeBurnlosses \%} = \frac{\text{estimate} - \text{real losses}}{\text{real losses}} 100 \tag{4.2}$$

In figures 4.33, 4.34, and 4.35 it is shown the results for the expression (4.2) for a specific impulse of 300 s for each steering type. If the estimation is similar to the real losses, we would expect a behavior where the predicted losses would be in percentage somewhat constant to the real losses. Instead in figures 4.33 and 4.34 we obtained similar results with a linear behavior in some cases (for low Δv maneuvers, apogee targeting) and in other cases exponential behavior (for high Δv maneuvers, C3 targeting). This may suggest the expression, despite giving above estimates for those cases, around $125\,\%$, it is not that reliable. Furthermore, the expression does not predict well for the case of constant thrust direction (figure 4.35), where it is only good in a small region of T/W_0 (0.1 to 0.25) just for the case of high Δv.

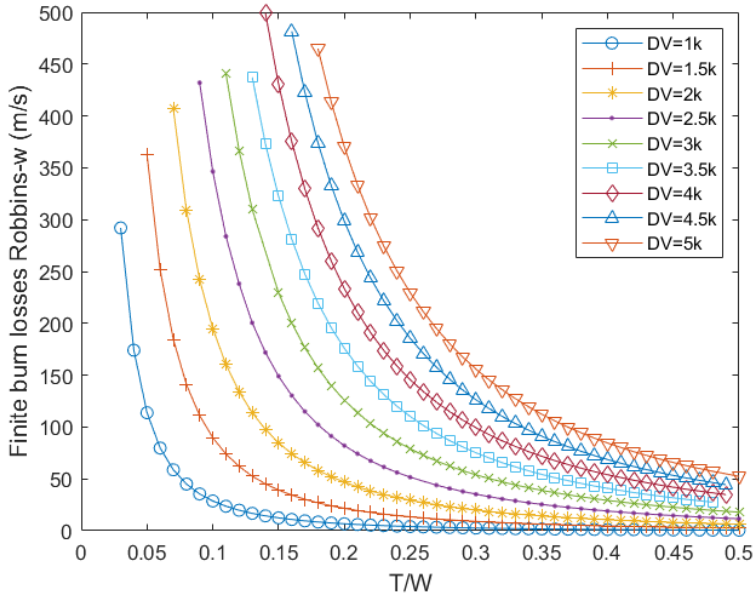

Figure 4.30: Difference between analytic estimation and numerical finite burn losses for intertial constant rotation thrust direction

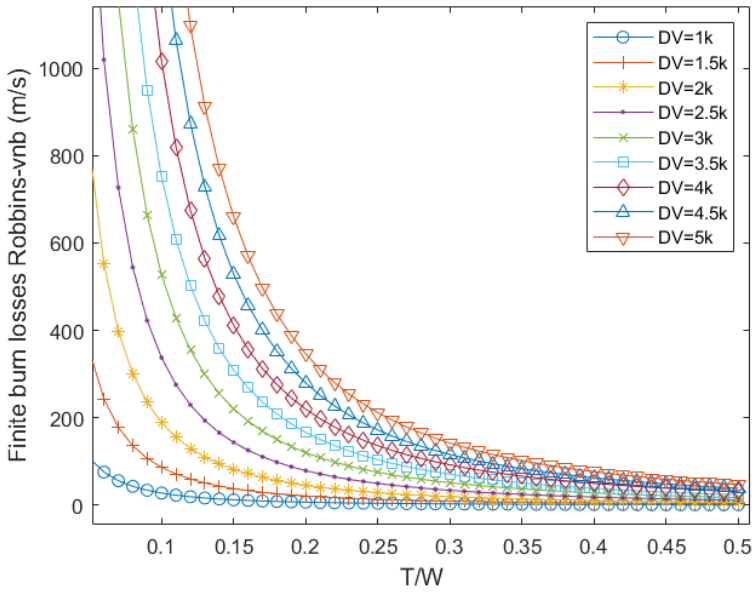

Figure 4.31: Difference between analytic estimation and numerical finite burn losses for thrust direction parallel to velocity for a specific impulse of 300 s

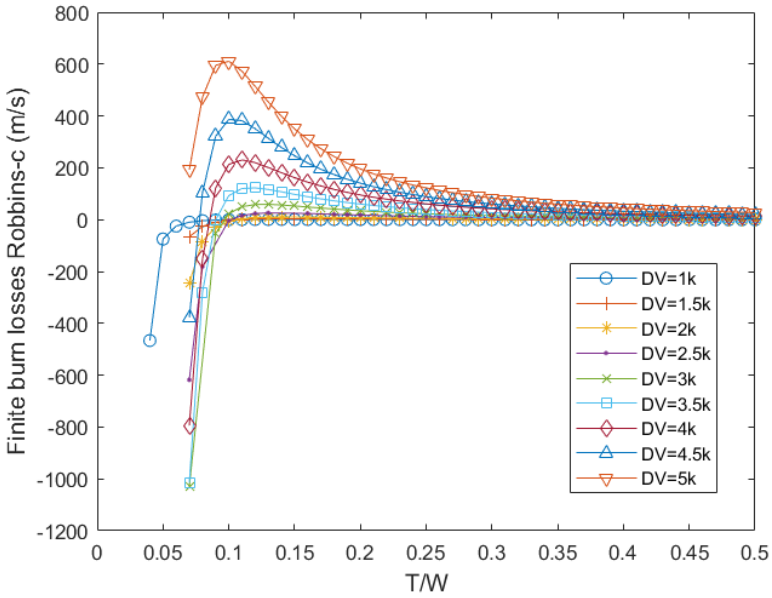

Figure 4.32: Difference between analytic estimation and numerical finite burn losses for inertial constant thrust direction for a specific impulse of 300 s

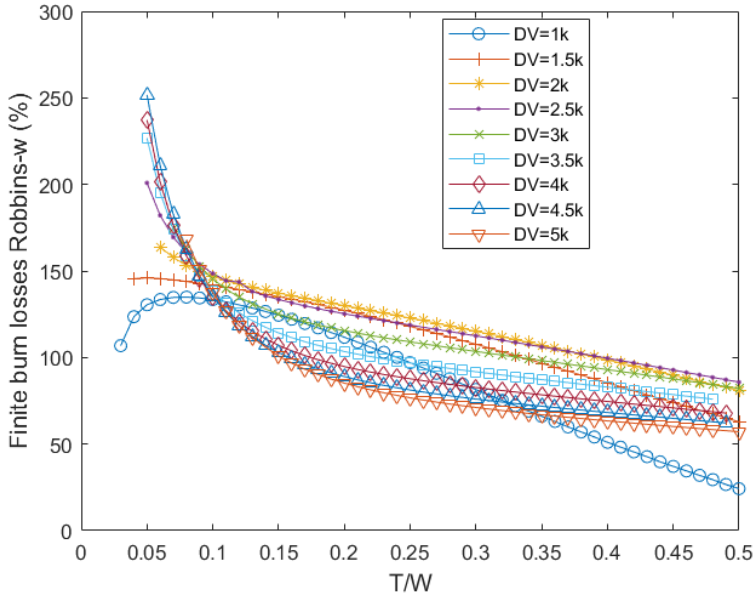

Figure 4.33: Difference between analytic estimation and numerical finite burn losses for intertial constant rotation thrust direction for a specific impulse of 300 s

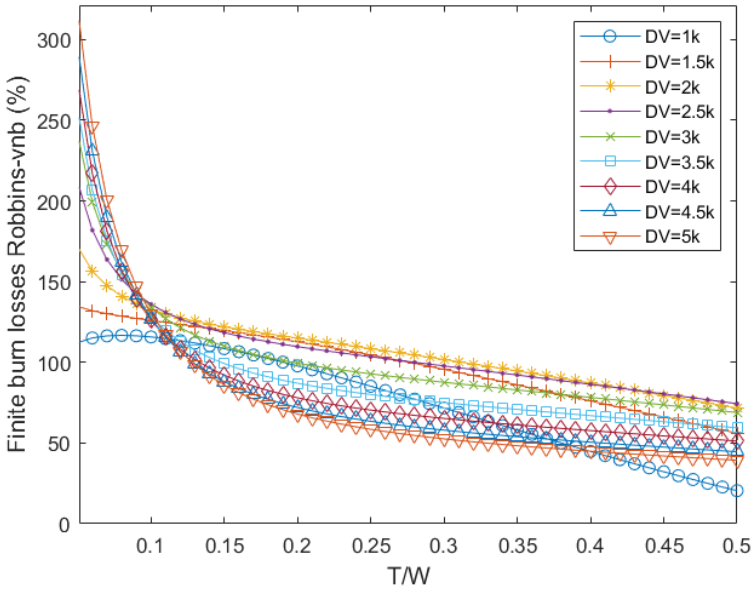

Figure 4.34: Difference between analytic estimation and numerical finite burn losses for thrust direction parallel to velocity for a specific impulse of 300 s

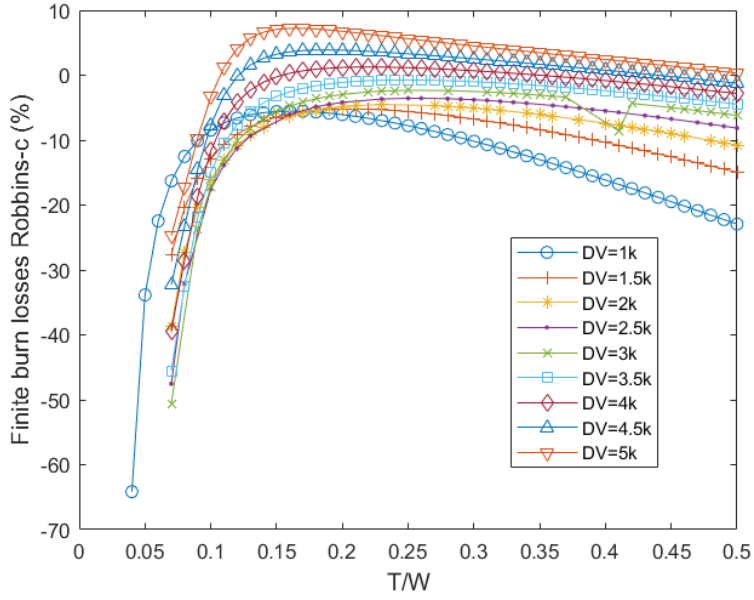

Figure 4.35: Difference between analytic estimation and numerical finite burn losses for inertial constant thrust direction

Figures 4.36, 4.37, 4.38, 4.39, and 4.40 show the results for specific impulse 250 s, 400 s, and 600 s, and for a specific impulse of 300 s starting from a circular orbit for different altitudes of 1000 km, and 5000 km. The altitude of 5000 km was chosen based on the gravity acceleration in Mars at an altitude of 300 km, where typically probes orbit. We can see that for all of the above scenarios, for thrust parallel to velocity the formula is always an upper bound to the losses.

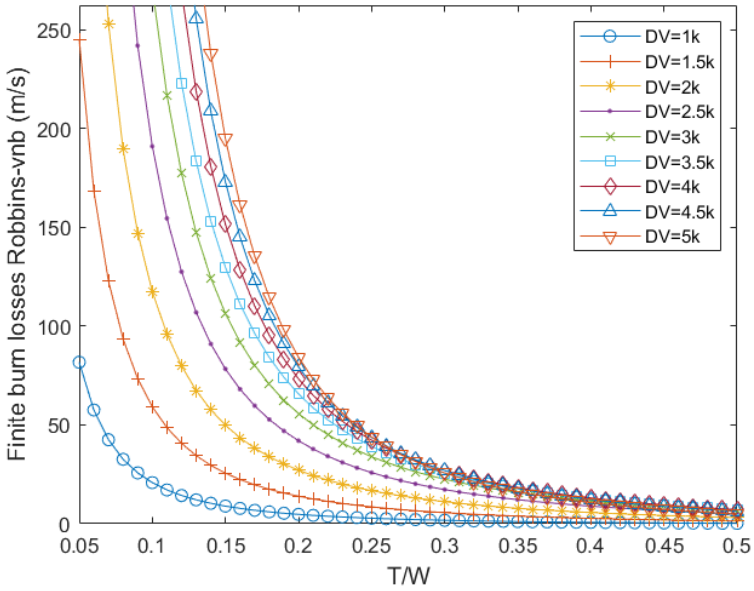

Figure 4.36: Difference between analytic estimation and numerical finite burn losses for specific impulse of 250 s for thrust parallel to velocity

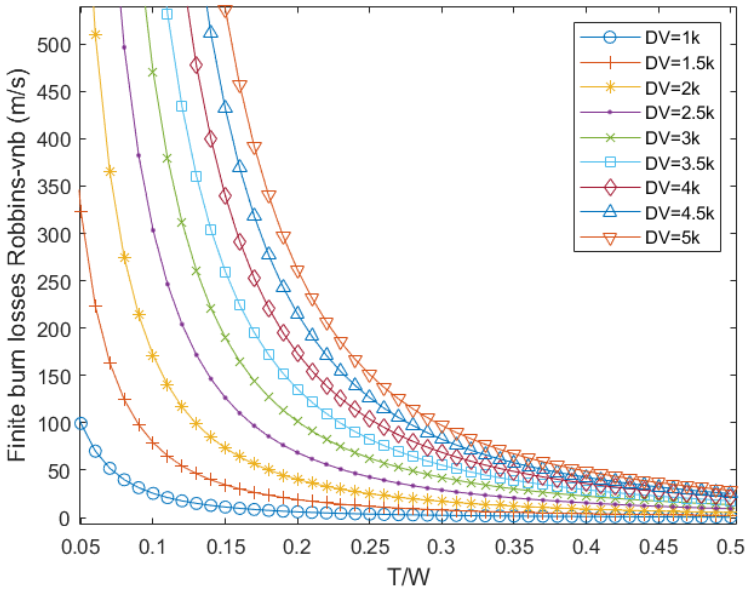

Figure 4.37: Difference between analytic estimation and numerical finite burn losses for specific impulse of 400 s for thrust parallel to velocity

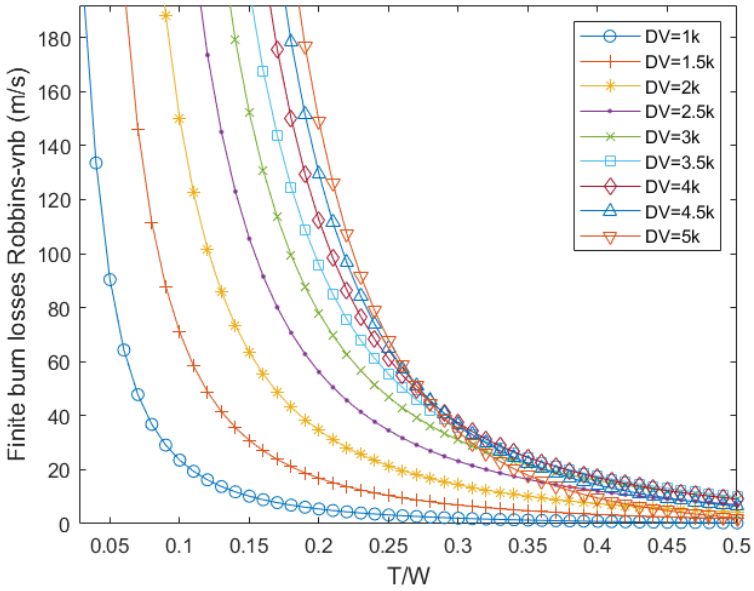

Figure 4.38: Difference between analytic estimation and numerical finite burn losses for specific impulse of 600 s for thrust parallel to velocity

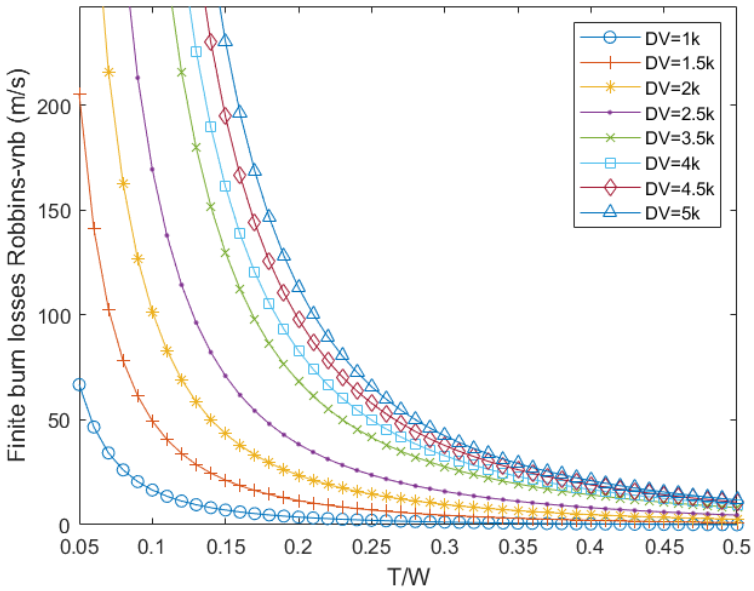

Figure 4.39: Difference between analytic estimation and numerical finite burn losses for specific impulse of 300 s and altitude of 1000 km for thrust parallel to velocity

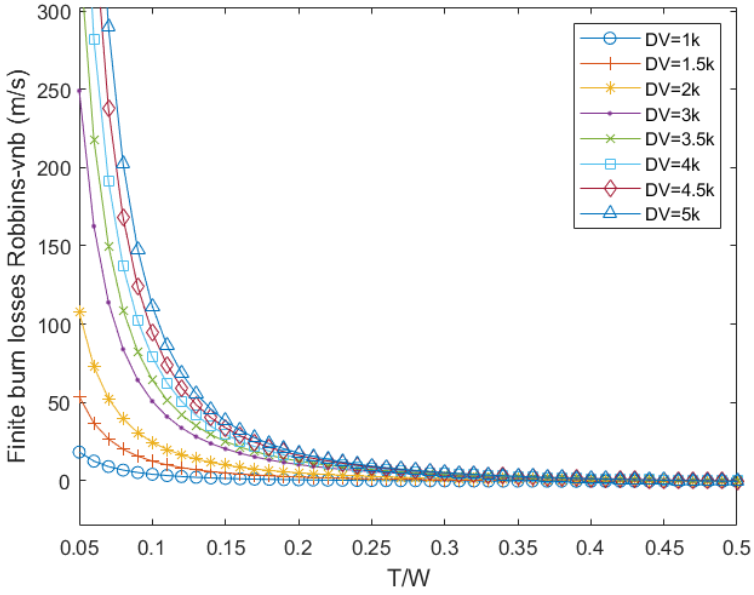

Figure 4.40: Difference between analytic estimation and numerical finite burn losses for specific impulse of 300 s and altitude of 5000 km for thrust parallel to velocity

4.2 Discussion of the results

All the cases exhibit the same pattern for the finite burn losses. They highly increase for smaller T/W_0 (around 0.1), whereas for higher T/W_0 (above 0.4) the curves are quite close to each other, as the duration of the maneuvers are shorter and the steering law has less effect on the losses (figures 4.2, 4.3, and 4.1). Of the three steering cases considered, constant thrust direction has the worst performance while constant thrust rotation and thrust parallel to velocity have similar losses. This is an important conclusion, because simulating thrust parallel to velocity is easier than optimizing a constant thrust rotation, and can be used as a first estimate for the losses in early mission design stages at least for T/W_0 not too small.

Comparing different specific impulses, we can see that higher specific impulses result in higher losses for the same ratio of T/W_0. However, sice the simulations were made with the same initial mass, the higher specific impulse case carries more dry mass. This happens because we are comparing cases for the same T/W_0. Whenn we compare different specific impulses for the same dry mass we observe smaller burn losses for higher specific impulses, and therefore a higher T/W_0 at launch. The approximation from the literature [14], (2.17), is confirmed to be an upper bound for the cases of constant rotation ad thrust parallel to velocity, overestimating the losses by 125 % for T/W_0 above 0.1, figures 4.34, and 4.33. For lower T/W_0, the maneuvers are long and can no longer be considered impulsive, being beyond the limits of validity of the upper bound. The expression is an upper bound but exceeds the real value considerably, which is good for risk mitigation but no so much for an estimate.

Chapter 5

Results for multiple apogee raising maneuver

In this chapter, the finite burn losses obtained from the alternative of multiple apogee raising maneuver are studied for a transfer orbit to mars and a geostationary transfer orbit.

5.1 Real burn losses on multiple apogee raising maneuver

The goal is to take advantage of the Oberth effect by having multiple maneuvers executed at low altitudes instead of a direct one that goes further away from the main body during its execution. Thus, it is important to analyze each perigee of the maneuvers, because the closer to the main body the better. Figure 4.19 from the previous chapter, where the perigee is studied for direct maneuvers for constant thrust direction, shows that it is the only steering case in which the perigee is closer to the main body. So, a priori, there is an interesting phenomenon at play where, on the one hand, it is the least effective steering law, on the other hand, it allows for the spacecraft to be closer to the main body thus suggesting it takes better advantage of multiple maneuvers. However, with constant rotation, such results could also be obtainable because the constant direction is the case where the rotation is $0\,\mathrm{rad/s}$.

On the table 5.1 results for the finite burn losses of multiple apogee raising maneuver to Mars are shown. As expected the best performance is for constant rotation where, as explained in the previous chapter, it can achieve both steering effectiveness and proximity to the main body. Although, we can see that constant direction has a better improvement over the other two.

It is important to note that these results may be local optima. With two forces at play here, the Oberth effect and the steering effectiveness, it is less trivial to analyze the results and conclude whether they are local optimum results. Nonetheless, the results obtained were analyzed (the optimal variables such as the beginning of the burn, the angles, and rotation) and we can state that at the very least they are realistic optima and thus acceptable for analysis.

5.1.1 Mars transfer orbit

We analyzed a case study of a crewed mission to Mars (where we want to spend the least Δv possible). The spacecraft may be large and thus have low maneuverability, and uses constant thrust direction as steering.

A maneuver to Mars at the starting orbit requires an impulsive approximation Δv of $3.6127\,\mathrm{km/s}$ to achieve the elliptical Hohmann transfer orbit. A specific impulse of $300\,\mathrm{s}$ and $T/W_0 = 0.15$ was used to obtain these results because they are conservative according to the existing technology from the Human Exploration of Mars Design Reference Architecture 5.0 [30]. On this Mars mission design, the trans-Mars insertion maneuver is planned to be done with 2 burns (1 extra burn in relation to a direct maneuver).

The table 5.1 shows the burn losses of multiple apogee raising maneuver to Mars and figure 5.1 shows in percentage the performance gained relative to the direct maneuver for the cases of constant direction and thrust parallel to velocity. From table 5.1 and figure 5.1, we see that for multiple maneu-

Table 5.1: finite burn losses of multiple apogee maneuvers to Mars

Maneuvers	Constant direction	Constant rotation	Thrust parallel to velocity
Direct	4047.12 m/s	3811.91 m/s	3824.95 m/s
1 extra	3719.67 m/s	3667.94 m/s	3676.68 m/s
2 extra	3660.45 m/s	3638.03 m/s	3644.90 m/s
3 extra	3640.58 m/s	n/a	3631.34 m/s

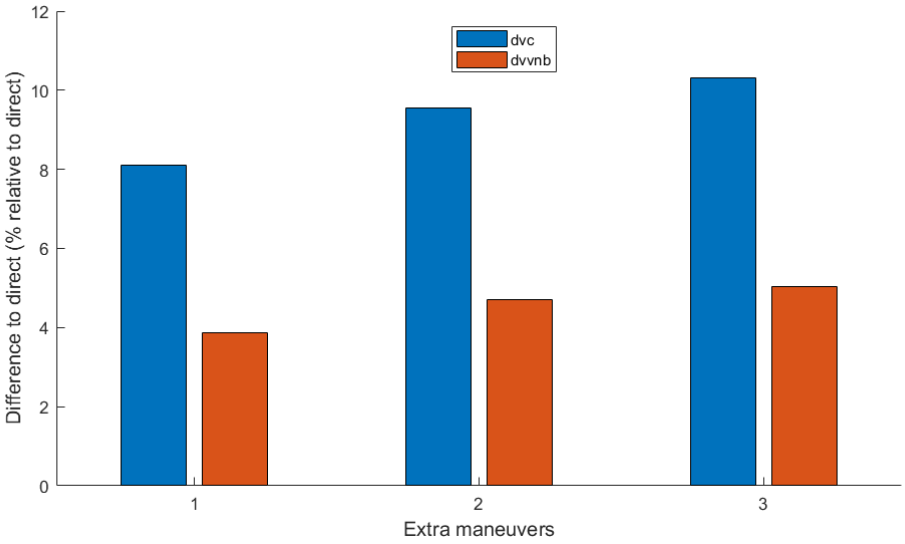

Figure 5.1: Δv difference in percentage relative to the direct escape maneuver for 1, 2, and 3 apogee raising maneuvers followed by the escape maneuver for the cases of constant rotation and thrust parallel to velocity.

vers, the more apogees raising are performed, the steering losses become more and more negligible. The initial difference of a direct maneuver of $4047\,\mathrm{m/s}$ versus $3824\,\mathrm{m/s}$ became just of $9\,\mathrm{m/s}$ at three extra maneuvers. In fact, the case of constant direction gains a lot more from multiple maneuvers than the other cases, reaching a $10\,\%$ efficiency with three extra maneuvers in relation to the direct maneuver, whereas the thrust parallel to velocity case gains close to $4\,\%$ and is stabilizing, as seen in figure 5.1. This indicates that it is a good orbit design option to make multiple maneuvers for a crewed Mars mission, especially if constant thrust direction is used (a single extra burn already saves $8\,\%$ Δv). Of course the more burns the more complex the orbit design becomes, and as planned on the reference 5.0 mission design [30] one extra maneuver may be enough for saving sufficient Δv.

Tables 5.2 and 5.3 show the perigee and the apogee of each apogee raising orbit respectively for three extra burns. It is interesting to observe that for the constant direction case the perigee remains lower and the apogee increases with maneuvers. Which means more energy was put into the elliptical orbits, whereas for thrust parallel to velocity the opposite happens. For the last case, we can hypothesize that it is related to better efficiency being put in the last maneuver as the steering is better. It is important to note that it is impossible to lower the perigee during the maneuver if we use thrust parallel to velocity because the semi-major axis is always increasing.

For constant direction, the perigee of the last maneuver is lower than of the previous one (the difference is just around $80\,\mathrm{m}$, but the other steering case increases in the order of $4\,\mathrm{km}$, suggesting that for the last maneuver the Oberth effect had more impact in obtaining better efficiency. This makes sense since the steering is not very effective. Figure 5.2 shows the orbits and the direction of the thrust on each one (the vectors) , all pointing inside.

Table 5.2: Perigee of constant direction and thrust parallel to velocity for 3 extra burns

Maneuver	1st perigee	2nd perigee	3rd perigee
constant direction	6570.90 km	6580.41 km	6580.33 km
thrust parallel to velocity	6578.14 km	6583.57 km	6587.50 km

Table 5.3: apogee of constant direction and thrust parallel to velocity for 3 extra burns

Maneuver	1st apogee	2nd apogee	3rd apogee
constant direction	9391.03 km	15519.46 km	38712.64 km
thrust parallel to velocity	8975.37 km	13128.76 km	21797.45 km

Table 5.4: orbital elements

Maneuvers	orbital element	1	2	3
Constant thrust	e	0.1767	0.4045	0.7094
	a	7980 km	11050 km	22646 km
parallel to velocity	e	0.1541	0.3320	0.5358
	a	7777 km	9856 km	14192 km

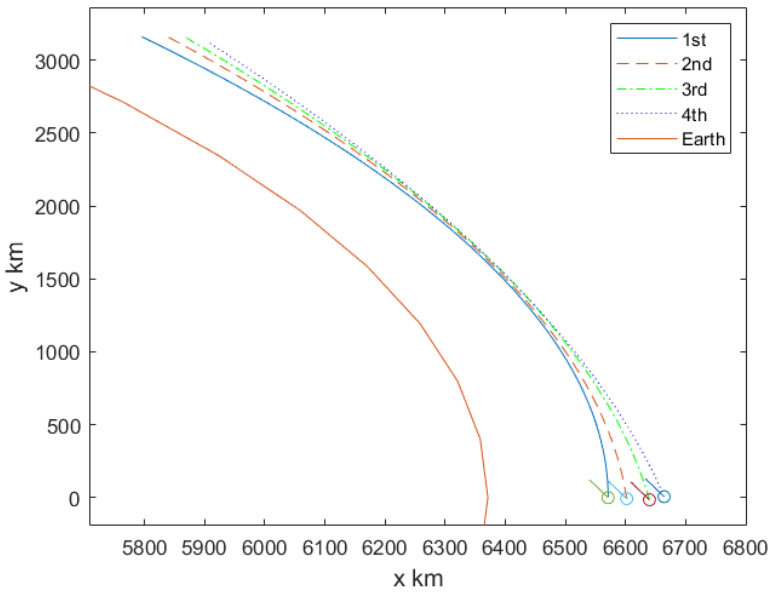

Figure 5.2: Amplified view on the 3 extra maneuvers for constant direction

For the other extra maneuvers:

Table 5.5: apogee and perigee for 2 extra burns

Maneuvers	perigee 1	perigee 2	apogee 1	apogee 2
Constant thrust	6571.09 km	6577.61 km	10875.39 km	26157.91 km
Constant rotation	6614.74 km	6647.09 km	13818.07 km	35188.21 km
Parallel to velocity	6584.51 km	6594.16 km	9788.74 km	16619.88 km

Table 5.6: semi-major axis and eccentricity for 2 extra burns

Maneuvers	orbital element	1	2
Constant thrust	e	0.2467	0.5982
	a	8723 km	16367 km
constant rotation	e	0.3525	0.6822
	a	10216 km	20918 km
parallel to velocity	e	0.1957	0.4319
	a	8187 km	11607 km

Table 5.7: apogee and perigee for 1 extra burn

Maneuvers	perigee 1	apogee 1
Constant thrust	6560.06 km	13816.65 km
Constant rotation	6629.40 km	15399.69 km
Parallel to velocity	6701.89 km	20171.56 km

Table 5.8: semi-major axis and eccentricity for 1 extra burn

Maneuvers	orbital element	1
Constant thrust	e	0.3561
	a	10188 km
constant rotation	e	0.3981
	a	11015 km
parallel to velocity	e	0.5012
	a	13437 km

5.2 Additional results on multiple maneuvers

Figure 5.3 shows the orbits of one extra maneuver for a case of constant rotation, where the vectors represent the thrust direction. We can observe the first maneuver starts with thrust pointing inside, misaligned with the velocity, and on the second it looks like it is almost aligned with the velocity. This suggests the first maneuver tries to get closer to the main body while the second maximizes the steering effectiveness.

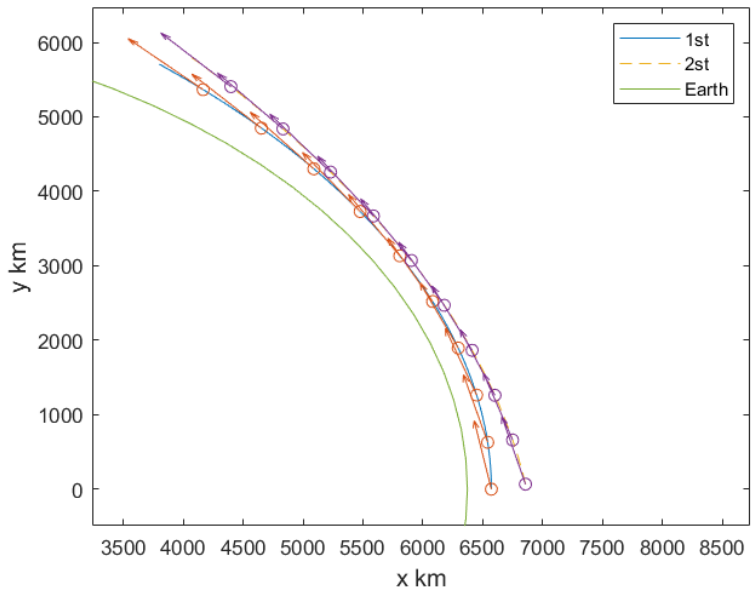

Figure 5.3: Amplified view on 1 extra maneuvers for constant rotation

It is also of interest to study how the total Δv affects the intermediate apogees and perigees. Figures 5.4 and 5.5 show the perigees and apogees for various Δv for extra 5 maneuvers. As the Δv gets higher

the perigee tends to move closer to the main body while the apogee gets significantly lower (less energy is being put into the elliptical orbits). Most probably to take advantage of the Oberth effect on the last maneuver as it gets longer with higher Δv. The effect of burn time being longer on the last maneuver is not observable in figure 5.2, because it is a small Δv, 3.6 compared to 8, where the last elliptical orbit should allow the escape maneuver to take advantage of the Oberth effect, thus being closer. Of course, these cases are for thrust parallel to velocity, in which the perigee always increases no matter what.

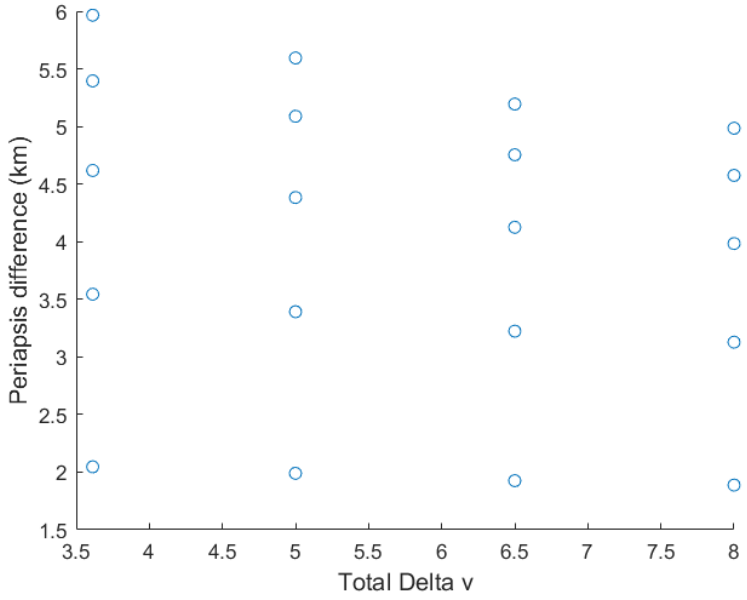

Figure 5.4: Perigees for different Δv for thurst parallel to velocity. For each Δv there are 5 perigees, the first one being the lowest

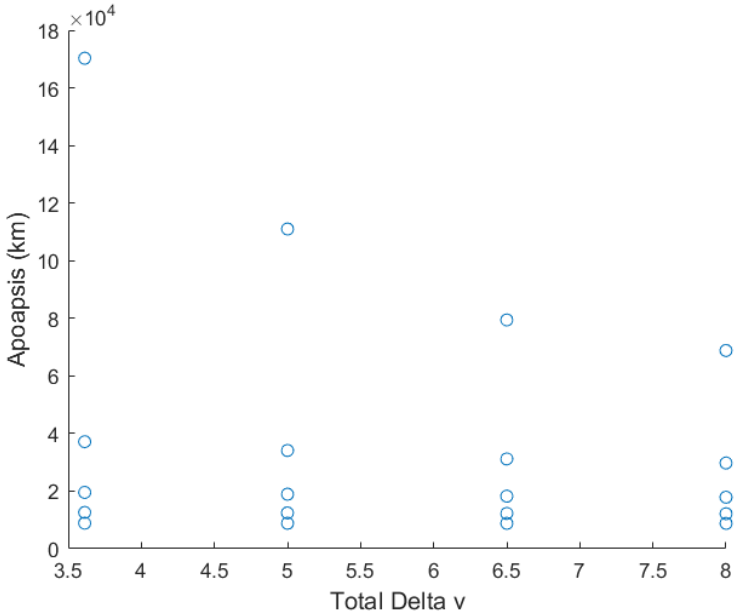

Figure 5.5: Apogees for different Δv for thurst parallel to velocity. For each Δv there are 5 apogees, the first one being the lowest

5.2.1 Geostationary Transfer Orbit

It was also determined multiple apogee raising maneuver for Geostationary Transfer Orbit (GTO). The GTO requires a impulsive approximation Δv of $2.3357\,\mathrm{km/s}$, the results obtained are presented on table 5.9. The aim of studying a GTO was to observe a case that is not an escape orbit and thus does not require a large maneuver at the end.

Again, constant direction with just one extra maneuver reduces the relative losses significantly relative to the other cases, by $5\,\%$ of the direct value whereas thrust parallel to velocity reduces around $1.4\,\%$. The optimizer could not find solutions for constant rotation with three extra maneuvers.

Table 5.9: finite burn losses of multiple apogee maneuvers to Geostationary orbit

Maneuvers	Constant direction	Constant rotation	Thrust parallel to velocity
Direct	2512.33 $\mathrm{m/s}$	2405.45 $\mathrm{m/s}$	2408.79 $\mathrm{m/s}$
1 extra	2378.76 $\mathrm{m/s}$	2354.75 $\mathrm{m/s}$	2373.03 $\mathrm{m/s}$
2 extra	2359.16 $\mathrm{m/s}$	2345.08 $\mathrm{m/s}$	2347.08 $\mathrm{m/s}$
3 extra	2347.41 $\mathrm{m/s}$	n/a	2345.86 $\mathrm{m/s}$

Chapter 6

Conclusions

In this work burn losses of space maneuvers around the Earth were analyzed for a wide range of Δv, T/W_0 for representative specific impulses and three different steering laws. As expected the worst performing steering law is the one with constant thrust direction while the other two cases have similar performances. The attempt to predict the finite burn losses in a simple way is found to be nontrivial. The analytical estimate from [14] does not predict the losses reliably, especially for thrust with constant direction, being an upper bound to the losses for the other two cases. Although, it is still better than a blindfold guess, being around 125% of the finite losses value for the cases of thrust parallel to velocity and inertial fixed rotation. The multiple apogee raising maneuver lowers significantly the losses particularly for the case of constant thrust direction (where it is saved 10% of the direct maneuver losses with three extra burns), that may be useful for a future mission to Mars.

6.1 Achievements

This work shows that thrust parallel to velocity does not always have the best performance in comparison to optimal steering as stated in [13]. Thrust parallel to velocity, which is the easiest to compute, can be used to estimate the Δv in the early stages of orbit design since it has similar performance in relation to thrust with fixed rotation. Higher specific impulse does not result in lower losses for the same T/W_0, but spends less propellant mass. The analytic estimate from [14] predicts by an excess of 125% the cases, but its error is much larger for the case of constant thrust direction. The Oberth effect and the steering losses are nontrivial to study, showing interesting effects when comparing thrust parallel to velocity to constant rotation, where efficiency in the velocity increment and being closer to the main body are at play and relevant for real maneuvers. Finally, a crewed mission to Mars would benefit if it used multiple maneuvers, especially because a large spacecraft with constant direction steering reduces significantly the steering losses.

6.2 Future Work

The prediction of the burn losses by using non-linear regression can be tested. The analytic estimate (2.17) may have other approaches and solutions where we could have a better prediction for the burn time of the maneuver. Another SQP based algorithm could be used. Furthermore, it would be interesting to do a similar study but starting on an elliptical orbit because it allows for more degrees of freedom.

Bibliography

[1] J. R. W. Wiley J. Larson. *Space Mission Analysis and Design*. Space Technology Library. Microcosm, 3rd edition, 2005. ISBN 1881883108.

[2] ArianeSpace. Soyuz user manual, 2015. URL http://www.arianespace.com/wp-content/uploads/2015/09/Soyuz-Users-Manual-March-2012.pdf. Accessed 06/12/2019.

[3] United Launch Alliance. Atlas V user guide, 2010. URL https://www.ulalaunch.com/docs/default-source/rockets/atlasvusersguide2010.pdf. Accessed 06/12/2019.

[4] C. D. Brown. *Spacecraft Mission Design*. AIAA Education Series. American Institute of Aeronautics and Astronautics, 2nd edition, 1998. ISBN 1563472627,9781563472626.

[5] GMAT Development Team. General Mission Analysis Tool (GMAT) User Guide The GMAT Development Team. Technical report, 2012. URL http://gmat.sourceforge.net/docs/R2012a/help-letter.pdf.

[6] H. Oberth. *Ways to Spaceflight*. Number n.º 622 in NASA technical translation. National Aeronautics and Space Administration, 1972.

[7] G. R. Hintz. *Orbital Mechanics and Astrodynamics: Techniques and Tools for Space Missions*. 2015. ISBN 9783319094441. doi: 10.1007/978-3-319-09444-1.

[8] C. Ocampo. Finite Burn Maneuver Modeling for a Generalized Spacecraft Trajectory Design and Optimization System. *Annals of the New York Academy of Science*, 233:210–233, 2004. doi: 10.1196/annals.1311.013.

[9] NASA. Copernicus trajectory design and optimization system, 2019. URL https://www.nasa.gov/centers/johnson/copernicus/index.html. Accessed 05/08/2019.

[10] D. Eagle. Optimal Finite-burn Interplanetary Injection from Earth Orbit - File Exchange - MATLAB Central, 2020. URL https://www.mathworks.com/matlabcentral/fileexchange/42215-optimal-finite-burn-interplanetary-injection-from-earth-orbit?s{_}tid=prof{_}contriblnk. Accessed 24/07/2019.

[11] P. E. Gill, W. Murray, M. A. Saunders, and E. Wong. User's guide for SNOPT 7.7: Software for large-scale nonlinear programming. Center for Computational Mathematics Report CCoM 18-1, Department of Mathematics, University of California, San Diego, La Jolla, CA, 2018.

[12] C. Zee. Effect of Finite Thrusting Time in Orbital Maneuvers. *AIAA Journal*, 1(1):60–64, 1963. ISSN 0001-1452. doi: 10.2514/3.1469.

[13] E. A. Villis. Finite-thrust escape from and capture into circular and elliptic orbits. *NASA Lewis Research Center Cleveland, NASA Technical Note*, 1967.

[14] H. M. Robbins. An analytical study of the impulsive approximation. *AIAA Journal*, 4(8):1417–1423, 1966. doi: 10.2514/3.3687.

[15] C. A. Ocampo and D. V. Byrnes. Mission Design and Trajectory Optimization. *Encyclopedia of Aerospace Engineering. John Wiley Sons, Ltd.*, pages 1–24, 2010. doi: 10.1002/9780470686652.eae286.

[16] R. H. Battin. *An introduction to the mathematics and methods of astrodynamics, Revised Edition*. AIAA Education series. American Institute of Aeronautics and Astronautics, Inc., 1999. ISBN 1563473429,9781563473425.

[17] G. P. Sutton and O. Biblarz. *Rocket Propulsion Elements*. John Wiley & Sons, 7th ed edition, 2001. ISBN 9780471326427,0-471-32642-9.

[18] S. Kemble. *Interplanetary Mission Analysis and Design*. Springer Praxis Books - Astronautical Engineering. Springer-Verlag Berlin Heidelberg, 1 edition, 2006. ISBN 3540299130,9783540299134.

[19] H. Ronald. Sequential Quadratic Programming. University of Houston, 2019. URL `https://www.math.uh.edu/~rohop/fall_06/Chapter4.pdf`.

[20] J. Hardtla. Gamma Guidance for the Inertial Upper Stage /IUS/. In *Guidance and Control Conference*, Reston, Virigina, aug 1978. American Institute of Aeronautics and Astronautics. doi: 10.2514/6.1978-1292. URL `http://arc.aiaa.org/doi/10.2514/6.1978-1292`.

[21] J. G. Beerer and R. B. Roncoli. Mars Observer Trajectory and Orbit Design. *Journal of Spacecraft and Rockets*, 28(5):515–521, 1991.

[22] R. W. Orloff. *Apollo by the numbers*. NASA History Division, 2005. URL `https://history.nasa.gov/SP-4029/Apollo_18-24_Translunar_Injection.htm`. Accessed 09/09/2019.

[23] W. Sidney and W. Lee. Mars Global Surveyur mission plan, 2019. URL `http://www.msss.com/mars/global_surveyor/mgs_msn_plan/section5/section5.html#RTFToC1`. Accessed 09/09/2019.

[24] P. Sivac and T. Schirmann. Information on Venus express orbiter, 2019. URL `https://sci.esa.int/documents/34571/36233/1567256526094-SivacWeb.pdf`. Accessed 06/12/2019.

[25] W. Sidney and W. Lee. Mars global surveyor mission planning, 2019. URL `http://www.msss.com/mars/global_surveyor/mgs_msn_plan/section2/section2.html#RTFToC23`. Accessed 06/12/2019.

[26] NASA. Cassini mission facts, 2019. URL https://solarsystem.nasa.gov/missions/cassini/mission/quick-facts/. Accessed 06/12/2019.

[27] Spaceflight101. spacecraft information INSAT-3D, 2019. URL http://spaceflight101.com/spacecraft/insat-3d/. Accessed 06/12/2019.

[28] J. J. Pocha. *An Introduction to Mission Design for Geostationary Satellites*. Springer Netherlands. ISBN 9789401082150. doi: 10.1007/978-94-009-3857-1.

[29] V. Sundararajan. Overview and technical architecture of india's Chandrayaan-2 mission to the moon. *AIAA Aerospace Sciences Meeting, 2018*, (210059):1–12, 2018. doi: 10.2514/6.2018-2178.

[30] G. T. Bagni. *Human Exploration of Mars Design Reference Architecture 5.0*. Number July. 2009. ISBN 3016210134.

Appendix A

Applying non-linear regression

By applying a non-linear regression of the type

$$ax^b \tag{A.1}$$

where a and b are the coefficients we are looking for, we obtain reasonable good fits as seen on the following figures for Isp of 300 s with the respective values for the coefficients.

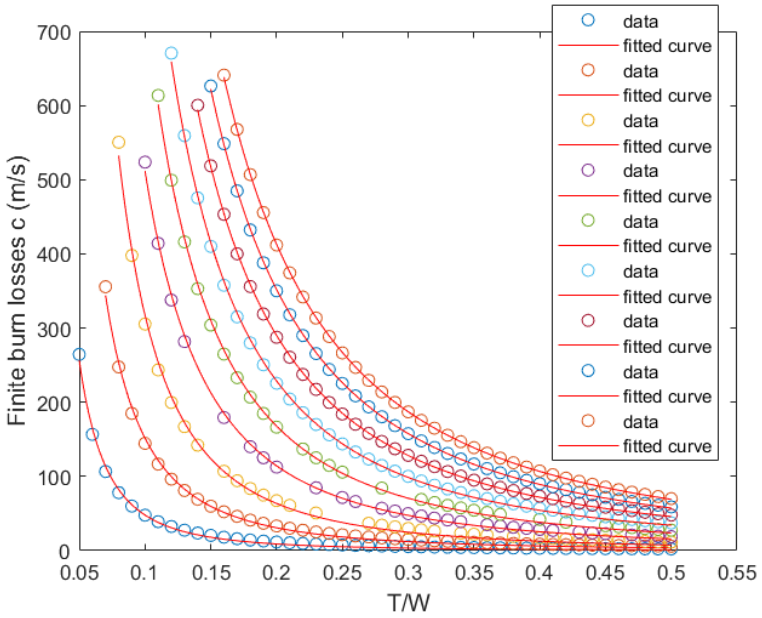

Figure A.1: Non-linear regression of the finite burn losses for inertial constant thrust direction. The impulsive Δv used are the same presented in this work

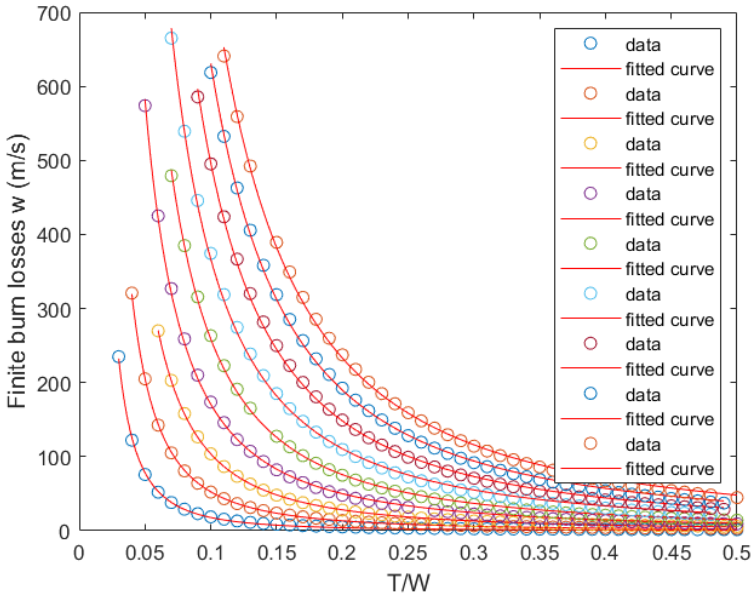

Figure A.2: Non-linear regression of the finite burn losses for inertial constant thrust rotation. The impulsive Δv used are the same presented in this work

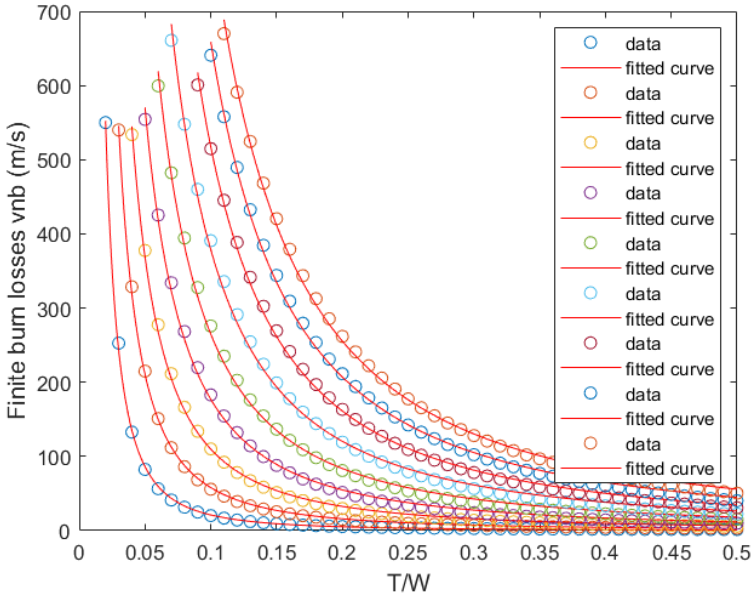

Figure A.3: Non-linear regression of the finite burn losses for thrust parallel to velocity. The impulsive Δv used are the same presented in this work

Table A.1: Regression coefficients for constant thrust direction

Δv km/s	a	b
1	0,182621418140826	-2,41930724816744
1,5	0,763263147525853	-2,29801031373019
2	1,51934594448177	-2,31977027038227
2,5	3,51391624132962	-2,16330356239076
3	5,41036045549786	-2,13421718767356
3,5	8,13884744357765	-2,07257393258770
4	11,3815468443650	-2,01194000597137
4,5	14,5570803950671	-1,97935228451181
5	17,8752386129935	-1,95102673408495

Table A.2: Regression coefficients for constant thrust rotation

Δv km/s	a	b
1	0,132200921417705	-2,13110625017184
1,5	0,562922830294186	-1,97006126532417
2	1,37693672274018	-1,87680166005664
2,5	2,89737509432496	-1,77012536602349
3	4,37513971591393	-1,77188554346343
3,5	6,88849104294620	-1,72605582753289
4	8,96540322098883	-1,74338761298321
4,5	11,6872205118809	-1,73216838944494
5	14,5995519615021	-1,72159489712090

Table A.3: Regression coefficients for thrust parallel to velocity

Δv km/s	a	b
1	0,198912812110450	-2,02687274555810
1,5	0,795624777138190	-1,86234268653217
2	1,96200418676623	-1,74796968143928
2,5	3,62644144402899	-1,68840509139904
3	5,77135661437468	-1,66185128445103
3,5	8,40823447597558	-1,65352224693844
4	10,7538488523413	-1,68223928897934
4,5	14,0878065219998	-1,66999084089922
5	17,6756865413055	-1,65940848887998